

Why calcite can be stronger than quartz

Journal Article**Author(s):**

Mancktelow, Neil S.; Pennacchioni, Giorgio

Publication date:

2010-01-20

Permanent link:

<https://doi.org/https://doi.org/10.3929/ethz-c-000017315>

Rights / license:

[In Copyright - Non-Commercial Use Permitted](#)

Originally published in:

Journal of Geophysical Research: Solid Earth 115(B1), <https://doi.org/10.1029/2009JB006526>



Why calcite can be stronger than quartz

Neil S. Mancktelow¹ and Giorgio Pennacchioni²

Received 9 April 2009; revised 12 August 2009; accepted 8 September 2009; published 20 January 2010.

[1] In the Neves area (Eastern Alps), calcite forms asymmetric centimeter-scale single-crystal porphyroclasts in quartz mylonites developed during hydrous amphibolite facies metamorphism at $\sim 550^\circ\text{C}$. Under these conditions, coarse calcite was clearly stronger than the surrounding polycrystalline, dynamically recrystallized, quartz matrix. Experimental results indicate that coarse calcite is less strain rate sensitive than wet quartzite, consistent with an inversion in strength on extrapolation to natural strain rates. For this to occur, wet quartzite must be weak, flowing at differential stress of <10 MPa. The lack of high-temperature twins (showing bulging or recrystallization) in calcite clasts is consistent with such low stresses during shear zone development under near peak metamorphic conditions. The maximum effective viscosity ratio of coarse calcite to quartzite for these conditions is probably not large (<10). However, numerical modeling shows that ratios of around 2 are sufficient to maintain near rigid calcite clast behavior for power law rheology with stress exponents appropriate to quartz ($n \sim 3-4$) and coarse calcite ($n \geq 6$). The inversion in relative strength reflects the difference in influence of water on the crystal plastic flow of calcite and quartz: water has a dramatic effect for quartz but little or no effect for calcite. Quartz-rich rocks under hydrous amphibolite facies conditions in the middle to lower crust are therefore relatively weak (in fact, weaker than coarse calcite) and flow at much lower stresses than dry quartz-rich rocks at similar crustal levels.

Citation: Mancktelow, N. S., and G. Pennacchioni (2010), Why calcite can be stronger than quartz, *J. Geophys. Res.*, *115*, B01402, doi:10.1029/2009JB006526.

1. Introduction

[2] Calcite and quartz are two of the most common minerals in the continental crust and understanding their mechanical behavior under geological conditions is critical for modeling crustal dynamics. It is therefore not surprising that these minerals have been extensively studied since the very beginning of laboratory rock mechanics experiments. However, extending such laboratory data to geological deformation rates in the range 10^{-10} – 10^{-14} s^{-1} [e.g., Pfiffner and Ramsay, 1982; Herwegh *et al.*, 2005; Sassier *et al.*, 2009] requires an extrapolation of around 4–10 orders of magnitude, with correspondingly large uncertainties [e.g., Paterson, 1987]. Observations of deformed natural rocks exhumed from depth in mountain belts are therefore crucial for providing independent constraints on the validity of this extrapolation.

[3] Brodie and Rutter [2000] note that extrapolation of experimental results for creep of calcite and quartz to natural deformation rates and temperatures under which both minerals are capable of ductile flow (>280 – 300°C) suggests that calcite marble should be of similar strength or even stronger than quartzite. However, they note that field observations generally indicate that quartz is significantly stronger than calcite in natural rocks, with quartz forming

barely deformed clasts in calcite marble mylonites [e.g., Bestmann *et al.*, 2004], or with quartzite layers being folded or boudinaged within a weaker calcite marble matrix. Brodie and Rutter [2000] argue that this contradiction can be explained if the effect of grain size is considered. Calcite grains may either start small (e.g., the Solnhofen fine-grained limestone often used in experiments), or become small due to dynamic recrystallization. In this case, the deformation mechanism may change, with an increase in the strain rate sensitivity and a corresponding larger decrease in flow stress with extrapolation to slow natural deformation rates. If, as proposed by Brodie and Rutter [2000], quartz does not generally attain the small grain sizes necessary for an equivalent change in mechanism, then the observed natural case, with quartz generally stronger than calcite, could be explained.

[4] We present here the complementary natural situation to that considered by Brodie and Rutter [2000], namely, where calcite started as large grains prior to deformation and maintained this coarse grain size. For this field example from the Neves area (Eastern Alps), calcite was stronger than quartz and formed asymmetric porphyroclasts in high-strain shear zones developed under hydrous amphibolite facies conditions.

2. Geological Outline and Field Relationships

[5] The Neves study area lies in the southwestern corner of the Tauern Window in the Eastern Alps (Italy). The regional and local structural features are discussed in detail by Pennacchioni and Mancktelow [2007] and the location is

¹Department of Earth Sciences, ETH Zurich, Zurich, Switzerland.

²Department of Geosciences, University of Padua, Padua, Italy.

given in Figure 1 of Pennacchioni and Mancktelow. The dominant rock type is a pre-Alpine granodiorite, locally intruded by leucogranite and crosscut by aplite, pegmatite and basic dikes. A well-developed magmatic foliation is present in the granodiorite but there was no significant solid-state deformation prior to the Alpine orogeny. Peak Alpine metamorphic conditions in the Neves area were around 550–600°C, according to the oxygen isotope fractionation data of *Hoernes and Friedrichsen* [1974], and 0.35–0.75 GPa, based on the fluid inclusion studies of *Cesare et al.* [2001]. Geothermometry on synkinematic garnet-biotite pairs from mylonites in the Neves granodiorite, with biotite outlining the foliation, yields a wide range of values depending on the calibration, but the estimated temperatures are all consistently above 550°C (Table 1).

[6] Heterogeneous Alpine deformation under peak metamorphic conditions has produced a network of ductile shear zones nucleating on precursor fractures and compositional layers or boundaries [Pennacchioni and Mancktelow, 2007]. Widespread quartz veins including variable amounts of coarse-grained (>1 cm) calcite (Figure 1a), biotite and plagioclase formed at near peak metamorphic conditions [Cesare et al., 2001] and during all stages of the amphibolite facies shearing, indicating fluid-rich conditions throughout the deformation history. Some veins localized shear deformation or were transposed along the amphibolite facies garnet-biotite-bearing shear zones to form quartz mylonites [Pennacchioni and Mancktelow, 2007]. Original coarse-grained calcite crystals in these veins were disaggregated into single-crystal porphyroclasts within the quartz matrix (Figures 1 and 2), with the size typically in the range of one to a few centimeters (Figures 1b, 1c, 1d, and 2) but in some cases reaching several tens of centimeters (Figure 1e). Less commonly, single-crystal calcite porphyroclasts are observed in mylonitic sheared granodiorite (Figure 1f). The calcite porphyroclasts usually have a monoclinic sigmoidal shape, with the long axis making a small antithetic (or countershearing) angle to the foliation (Figures 1 and 2), a geometry typical of nonrotating porphyroclasts in mylonites [e.g., Mancktelow et al., 2002]. Overall, the field relationships in the Neves area unequivocally demonstrate that calcite was stronger than quartz (and granodiorite) during shearing under water-rich amphibolite facies conditions.

3. Composition, Microstructure, and Crystallographic Preferred Orientation

[7] Undeformed quartz veins are rare and typically consist of coarse grained blocky crystals on the centimeter scale (Figure 1a). The large majority of veins are deformed and quartz is finer-grained due to dynamic recrystallization. Quartz mylonites derived from veins shows a microstructure typical of deformation under amphibolite facies conditions (Figure 2b). The recrystallized quartz consists of millimeter-scale grains showing irregular lobate boundaries at the scale of hundreds of microns, characteristic of dynamic grain boundary migration [e.g., Urai et al., 1986]. This dynamic microstructure, with quite irregular grain boundaries, is preserved without evidence for significant subsequent grain growth or annealing. According to *Stipp et al.* [2002], grain boundary migration recrystallization in quartz starts to dominate at around 500–550°C.

[8] The crystallographic preferred orientation (CPO) of the quartz mylonites was investigated by X-ray texture goniometry. Given the coarse grain size of the quartz, analysis was carried out on a PANalytical system at the Geoscience Centre of the University of Göttingen (Germany), which is equipped with a polycapillary glass fiber lens at the primary beam side that provides high X-ray intensities, an optically parallel beam and an exceptionally large beam size of up to 7 mm. This setup results in a short measuring time per pole figure (1 s per pole figure direction at an anode current of 40 mA and a voltage of 40 kV), a high spectral resolution and a relatively large measuring area for each analysis spot (~1 cm²). The quartz mylonites have a strong CPO, with the *c* axes patterns ranging from an oblique partial girdle (Figure 3a), through a partial girdle about Y and slightly oblique to the Z direction (Figure 3b), to an almost single-crystal CPO with *c* axes preferentially parallel to Y (Figure 3c). In all cases, the strongest $\langle a \rangle$ maximum lies in the XZ plane perpendicular to the foliation (i.e., on the periphery of the stereo plots in Figure 3) at an angle of ~16–20° to the lineation, measured in a corotational sense with the (dextral) sense of shear. Such patterns, suggesting dislocation creep on the prism $\langle a \rangle$ or mixed prism and rhomb $\langle a \rangle$ systems, are typical for crystal plastic deformation of quartz under amphibolite facies conditions [e.g., Schmid and Casey, 1986; Stipp et al., 2002].

[9] In the field, the calcite typically has a tan to reddish brown weathering color (Figure 1). Electron microprobe analyses (Figure 4) show that calcite contains small amounts of FeO (2.4 wt %) and minor amounts of MgO (0.4 wt %) and MnO (0.6 wt %). The calcite porphyroclasts in the quartz mylonites are commonly single crystals, with the local development of large (several hundred microns to often millimeter scale) subgrains. In most clasts, recrystallization is very limited and restricted to the sigmoidal tails but some more elongate clasts have recrystallized to a mosaic of new millimeter-sized grains. The preservation of coarse subgrains and new grains, indicating limited recovery and recrystallization at high temperature and low differential stress, argues against a pervasive postdeformational overprint or annealing of the calcite microstructure. The single-crystal calcite porphyroclasts, isolated within amphibolite facies quartz mylonites, are strongly analogous to the single-crystal quartz porphyroclasts in a mylonitic calcite matrix described by *Bestmann et al.* [2004], which were deformed under greenschist facies conditions. In both cases, grains of the matrix develop a marked positive relief against the porphyroclast material, as is clearly seen both in casts of the porphyroclasts (Figure 1d) and in backscatter images under the SEM (Figure 4a).

[10] The crystallographic orientation of grains from 6 calcite porphyroclasts measured by X-ray texture goniometer is given in Figure 5. Although the number of data points is not sufficient for good statistics, the porphyroclasts apparently do not have a strong preferred orientation, even if the *c* axes are generally at a moderate to high angle to the foliation and lineation. Calcite porphyroclasts are therefore not in a specific “hard” orientation that could explain their resistance to deformation.

[11] As noted above, calcite porphyroclasts have irregular boundaries on a fine scale, with thin, discontinuous, optically dusty rims (Figure 2a). The irregular boundary is due

Table 1. Estimates of the Deformation Temperature in the Neves Mylonites Based on Coexisting Garnet and Biotite Compositions at 0.35 GPa and 0.75 GPa According to Different Calibrations^a

| | Garnet | | | | | | | | | |
|---------------------------------|---|----------------|----------------|----------------|----------------|---------------|--------------|--------------|---------------|--------|
| | gt3-2 (1) | gt3-14r (2) | gt3-14r (3) | gt3-15r (4) | gt3-16r (5) | gt3-17 (6) | gt4-1 (7) | gt4-2 (8) | gt2-7r (9) | |
| Fe ²⁺ | 1.95 | 1.96 | 1.96 | 1.95 | 1.93 | 2.00 | 2.01 | 1.99 | 1.99 | |
| Mg | 0.21 | 0.21 | 0.21 | 0.22 | 0.19 | 0.20 | 0.22 | 0.20 | 0.20 | |
| Mn | 0.06 | 0.05 | 0.05 | 0.06 | 0.07 | 0.04 | 0.05 | 0.05 | 0.05 | |
| Ca | 0.85 | 0.85 | 0.85 | 0.86 | 0.86 | 0.86 | 0.87 | 0.84 | 0.83 | |
| Almandine | 0.64 | 0.64 | 0.64 | 0.63 | 0.63 | 0.65 | 0.64 | 0.65 | 0.65 | |
| Pyrope | 0.07 | 0.07 | 0.07 | 0.07 | 0.06 | 0.06 | 0.07 | 0.07 | 0.07 | |
| Spessartine | 0.02 | 0.02 | 0.02 | 0.02 | 0.02 | 0.01 | 0.02 | 0.02 | 0.02 | |
| Grossular | 0.28 | 0.28 | 0.28 | 0.28 | 0.28 | 0.28 | 0.28 | 0.27 | 0.27 | |
| Fe/(Fe + Mg) | 0.90 | 0.91 | 0.91 | 0.90 | 0.91 | 0.91 | 0.90 | 0.91 | 0.91 | |
| Mg/(Fe + Mg) | 0.10 | 0.09 | 0.09 | 0.10 | 0.09 | 0.09 | 0.10 | 0.09 | 0.09 | |
| | Biotite | | | | | | | | | |
| | bt3-1 (1) | bt3-4r (2) | bt3-4b (3) | bt3-5 (4) | bt3-6 (5) | bt3-7 (6) | bt4-1 (7) | bt4-2 (8) | bt2-1 (9) | |
| Si | 5.573 | 5.504 | 5.516 | 5.489 | 5.520 | 5.536 | 5.656 | 5.638 | 5.534 | |
| Al IV | 2.427 | 2.496 | 2.484 | 2.511 | 2.480 | 2.464 | 2.344 | 2.362 | 2.466 | |
| Al VI | 0.559 | 0.652 | 0.667 | 0.638 | 0.639 | 0.620 | 0.645 | 0.593 | 0.622 | |
| total Al | 2.987 | 3.148 | 3.151 | 3.149 | 3.119 | 3.084 | 2.989 | 2.955 | 3.087 | |
| Ti | 0.283 | 0.229 | 0.204 | 0.235 | 0.251 | 0.204 | 0.243 | 0.239 | 0.181 | |
| Fe ²⁺ | 3.010 | 3.049 | 3.087 | 3.134 | 3.100 | 3.159 | 2.932 | 2.938 | 3.069 | |
| Mn | 0.050 | 0.045 | 0.048 | 0.059 | 0.044 | 0.041 | 0.041 | 0.029 | 0.048 | |
| Mg | 1.846 | 1.826 | 1.788 | 1.738 | 1.732 | 1.778 | 1.877 | 1.937 | 1.908 | |
| Ca | 0.000 | 0.013 | 0.005 | 0.022 | 0.005 | 0.001 | 0.000 | 0.000 | 0.002 | |
| K | 1.774 | 1.732 | 1.782 | 1.706 | 1.777 | 1.803 | 1.723 | 1.783 | 1.772 | |
| Na | 0.033 | 0.024 | 0.019 | 0.031 | 0.024 | 0.027 | 0.012 | 0.036 | 0.026 | |
| Fe/(Fe + Mg) | 0.620 | 0.625 | 0.633 | 0.643 | 0.642 | 0.640 | 0.610 | 0.603 | 0.617 | |
| Mg/(Fe + Mg) | 0.380 | 0.375 | 0.367 | 0.357 | 0.358 | 0.360 | 0.390 | 0.397 | 0.383 | |
| Phlogophite (Mn) | 0.321 | 0.315 | 0.309 | 0.299 | 0.300 | 0.306 | 0.327 | 0.338 | 0.327 | |
| Annite (Mn) | 0.524 | 0.526 | 0.533 | 0.540 | 0.538 | 0.544 | 0.511 | 0.512 | 0.527 | |
| X (Al IV) | 0.093 | 0.109 | 0.111 | 0.106 | 0.106 | 0.103 | 0.108 | 0.099 | 0.104 | |
| X (Mg) | 0.308 | 0.304 | 0.298 | 0.290 | 0.289 | 0.296 | 0.313 | 0.323 | 0.318 | |
| X (Fe) | 0.502 | 0.508 | 0.515 | 0.522 | 0.517 | 0.527 | 0.489 | 0.490 | 0.512 | |
| X (Ti) | 0.047 | 0.038 | 0.034 | 0.039 | 0.042 | 0.034 | 0.040 | 0.040 | 0.030 | |
| X (K) | 0.887 | 0.866 | 0.891 | 0.853 | 0.888 | 0.902 | 0.861 | 0.891 | 0.886 | |
| Phlogopite | 0.324 | 0.317 | 0.311 | 0.303 | 0.303 | 0.309 | 0.329 | 0.339 | 0.330 | |
| Annite | 0.528 | 0.530 | 0.537 | 0.546 | 0.542 | 0.548 | 0.515 | 0.515 | 0.531 | |
| LnKd (Grt-Bt) | 1.755 | 1.743 | 1.710 | 1.613 | 1.725 | 1.735 | 1.765 | 1.871 | 1.798 | |
| | Estimated Sample Temperature (°C) at P = 0.35 GPa | | | | | | | | | |
| | 1 | 2 | 3 | 4 | 5 | 6 | 7 | 8 | 9 | Mean T |
| Thomson [1976] | 578 | 581 | 590 | 616 | 586 | 583 | 575 | 549 | 567 | 581 |
| Goldman and Albee [1977a] | 520 | 522 | 528 | 546 | 525 | 523 | 518 | 500 | 512 | 522 |
| Goldman and Albee [1977b] | 564 | 574 | 584 | 610 | 577 | 568 | 574 | 539 | 557 | 572 |
| Holdaway and Lee [1977] | 568 | 570 | 578 | 601 | 574 | 572 | 565 | 542 | 558 | 570 |
| Ferry and Spear [1978] | 563 | 567 | 579 | 613 | 574 | 570 | 560 | 527 | 550 | 567 |
| Lavrent'eva and Perchuk [1981] | 590 | 592 | 599 | 617 | 596 | 594 | 588 | 569 | 582 | 592 |
| Hodges and Spear [1982] | 667 | 671 | 683 | 719 | 680 | 674 | 664 | 628 | 650 | 671 |
| Pigage and Greenwood [1982] | 746 | 750 | 763 | 808 | 764 | 752 | 741 | 698 | 724 | 749 |
| Perchuk and Lavrent'eva [1983a] | 596 | 599 | 605 | 624 | 602 | 600 | 595 | 575 | 588 | 598 |
| Perchuk and Lavrent'eva [1983b] | 587 | 590 | 596 | 615 | 593 | 591 | 586 | 566 | 579 | 589 |
| Perchuk and Lavrent'eva [1983c] | 569 | 572 | 578 | 596 | 575 | 573 | 568 | 549 | 562 | 571 |
| Ganguly and Saxena [1984a] | 636 | 641 | 653 | 687 | 654 | 648 | 630 | 598 | 621 | 641 |
| Ganguly and Saxena [1984b] | 634 | 639 | 652 | 685 | 652 | 646 | 628 | 597 | 620 | 639 |
| Perchuk et al. [1981] | 696 | 698 | 705 | 727 | 705 | 700 | 694 | 671 | 684 | 698 |
| Indares and Martignole [1985a] | 598 | 613 | 629 | 657 | 616 | 621 | 602 | 570 | 603 | 612 |
| Indares and Martignole [1985b] | 636 | 649 | 667 | 701 | 656 | 658 | 636 | 601 | 639 | 649 |
| Williams and Grambling [1990] | 765 | 769 | 784 | 830 | 784 | 773 | 759 | 715 | 742 | 769 |
| Dasgupta et al. [1991] | 614 | 614 | 624 | 655 | 617 | 619 | 610 | 583 | 606 | 616 |
| Bhattacharya et al. [1992] | 590 | 592 | 598 | 618 | 593 | 594 | 589 | 569 | 582 | 592 |
| Bhattacharya et al. [1992] | 544 | 545 | 551 | 570 | 542 | 547 | 545 | 526 | 539 | 545 |

Table 1. (continued)

| | Estimated Temperature (°C) at P = 0.75 GPa | | | | | | | | | Mean T |
|---------------------------------|--|-----|-----|-----|-----|-----|-----|-----|-----|--------|
| | 1 | 2 | 3 | 4 | 5 | 6 | 7 | 8 | 9 | |
| Thomson [1976] | 606 | 609 | 618 | 645 | 614 | 612 | 603 | 576 | 595 | 609 |
| Goldman and Albee [1977a] | 520 | 522 | 528 | 546 | 525 | 523 | 518 | 500 | 512 | 522 |
| Goldman and Albee [1977b] | 564 | 574 | 584 | 610 | 577 | 568 | 574 | 539 | 557 | 572 |
| Holdaway and Lee [1977] | 581 | 584 | 591 | 615 | 588 | 586 | 579 | 555 | 571 | 583 |
| Ferry and Spear [1978] | 579 | 583 | 594 | 629 | 589 | 585 | 575 | 541 | 564 | 582 |
| Lavrent'eva and Perchuk [1981] | 601 | 603 | 610 | 629 | 607 | 605 | 599 | 580 | 593 | 603 |
| Hodges and Spear [1982] | 681 | 685 | 697 | 734 | 694 | 688 | 678 | 641 | 664 | 685 |
| Pigage and Greenwood [1982] | 761 | 765 | 779 | 824 | 779 | 767 | 756 | 712 | 738 | 765 |
| Perchuk and Lavrent'eva [1983a] | 571 | 573 | 580 | 598 | 577 | 575 | 569 | 551 | 563 | 573 |
| Perchuk and Lavrent'eva [1983b] | 577 | 579 | 585 | 604 | 582 | 580 | 575 | 556 | 569 | 579 |
| Perchuk and Lavrent'eva [1983c] | 587 | 590 | 596 | 615 | 593 | 591 | 586 | 566 | 579 | 589 |
| Ganguly and Saxena [1984a] | 651 | 656 | 668 | 703 | 669 | 663 | 644 | 613 | 636 | 656 |
| Ganguly and Saxena [1984b] | 649 | 654 | 667 | 701 | 667 | 661 | 643 | 611 | 634 | 654 |
| Perchuk et al. [1981] | 727 | 730 | 737 | 759 | 737 | 732 | 726 | 702 | 715 | 729 |
| Indares and Martignole [1985a] | 612 | 627 | 643 | 671 | 630 | 635 | 616 | 583 | 617 | 626 |
| Indares and Martignole [1985b] | 651 | 664 | 682 | 717 | 672 | 674 | 651 | 616 | 654 | 664 |
| Williams and Grambling [1990] | 780 | 785 | 800 | 847 | 800 | 788 | 775 | 730 | 757 | 785 |
| Dasgupta et al. [1991] | 633 | 633 | 643 | 675 | 636 | 638 | 628 | 601 | 624 | 634 |
| Bhattacharya et al. [1992] | 592 | 595 | 601 | 621 | 595 | 596 | 592 | 571 | 585 | 594 |
| Bhattacharya et al. [1992] | 547 | 549 | 555 | 573 | 545 | 550 | 548 | 529 | 542 | 549 |

^aGarnet and biotite pairs and the corresponding estimates are reported within the same column (numbered 1–9). Results were calculated using the spreadsheet program of Rao [1995]. Original references for the different temperature calibrations are given with repeated references referring to different calibrations in the same publication (see Rao [1995] for details).

to interfingering with small quartz grains of the matrix, which also form isolated rounded inclusions (several tens to a few hundred microns in size) in the calcite rim (Figures 4a and 6). These quartz inclusions cut calcite twins (Figure 6). The calcite rim is crystallographically continuous with the single-crystal porphyroclast but can also include some new grains. The composition of the rim is almost pure calcite (Figure 4b), with micron-sized grains of a Mn-Fe-Si and Si-Fe-bearing phase irregularly dispersed along healed microcrack or cleavage planes. The markedly reduced solid solution of Fe, Mn, and Mg in the calcite rim suggests that it developed late in the retrograde history, under low-grade metamorphic conditions [Anovitz and Essene, 1987].

[12] Porphyroclasts contain both thin (Figure 6a) and thicker ($\leq 150 \mu\text{m}$, Figure 6b) straight twins, commonly forming two sets (Figures 2 and 6a). Following the nomenclature of Burkhard [1993], these are type II twins typically developed under temperatures of 150–300°C. The thin twins are quite sharp and discrete, but still have a recognizable width commonly $> 5 \mu\text{m}$ under the optical microscope. They are therefore still classified as type II rather than type I (which would be more typical of deformation $< 200^\circ\text{C}$ [Ferrill, 1991, 1998; Burkhard, 1993]). The twin boundaries are perfectly straight, without any evidence of bulging or recrystallization (Figure 6). Sutured twin boundaries and trails of small recrystallized grains are typical of type IV twins developed above 250°C [Burkhard, 1993; Ferrill et al., 2004]. The observed twins therefore could not have developed during shearing at peak metamorphic conditions (around 550°C) but instead formed later on the retrograde path, at temperatures below 250–300°C. The fact that twins are cut by quartz inclusions associated with the Fe-, Mg-, and Mn-poor porphyroclast rim (Figure 6) indicates that these inclusions developed during postkinematic modification of the original high-temperature porphyroclast-matrix interface. Twins are continuous from core to rim, so they must have formed after rim development, reflecting continued deformation under retrograde conditions.

[13] As noted above, the sigmoidal “sigma-clast” shape of the porphyroclasts indicates that they attained a stable orientation [Passchier and Simpson, 1986; Pennacchioni et al., 2001; Mancktelow et al., 2002], and Pennacchioni and Mancktelow [2007] have shown that the regional stress orientation in the Neves area did not change along the retrograde path. The orientation of the calcite single-crystal porphyroclasts relative to the principal stress axes has therefore remained effectively unchanged from peak amphibolite facies conditions to late faulting marked by the growth of chlorite and zeolite. Twins did develop under lower grade conditions, so the orientation of the clasts was not unfavorable for twinning. Rather, the lack of high-temperature twins must imply that the differential stress experienced by the single-crystal calcite grains during shearing under hydrous amphibolite facies conditions around 550°C was simply too low to produce twinning.

[14] Following Jamison and Spang [1976], twinning requires that $S_1 \Delta\sigma > t_c$, where S_1 is the “resolved shear stress coefficient” or “Schmid factor” and t_c the critical resolved shear stress (CRSS) for twinning. Taking the maximum possible value of 0.5 for S_1 (compare Jamison and Spang's Figure 4) and $t_c = 10 \text{ MPa}$ [Jamison and Spang, 1976; Tullis, 1980; Lacombe and Laurent, 1996; Ferrill, 1998], the differential stress must have been $< 20 \text{ MPa}$. Although the value of $t_c = 10 \text{ MPa}$ is often quoted and rather generally accepted, it should be noted that (1) the t_c values for e twinning of Turner et al. [1954, Table 1] are on the order of only 2–3 MPa for their highest temperature experiments at 300°C and (2) that t_c is also somewhat strain rate-dependent [de Bresser and Spiers, 1997], resulting in lower values under natural conditions. It follows that, although the analysis of Jamison and Spang [1976] assumes uniaxial stress and no CPO, both of which are not correct in our example, the value of 20 MPa should still represent a quite conservative upper limit. In the experiments of Rowe and Rutter [1990] in Carrara marble and a coarser-grained marble from Taiwan, the development

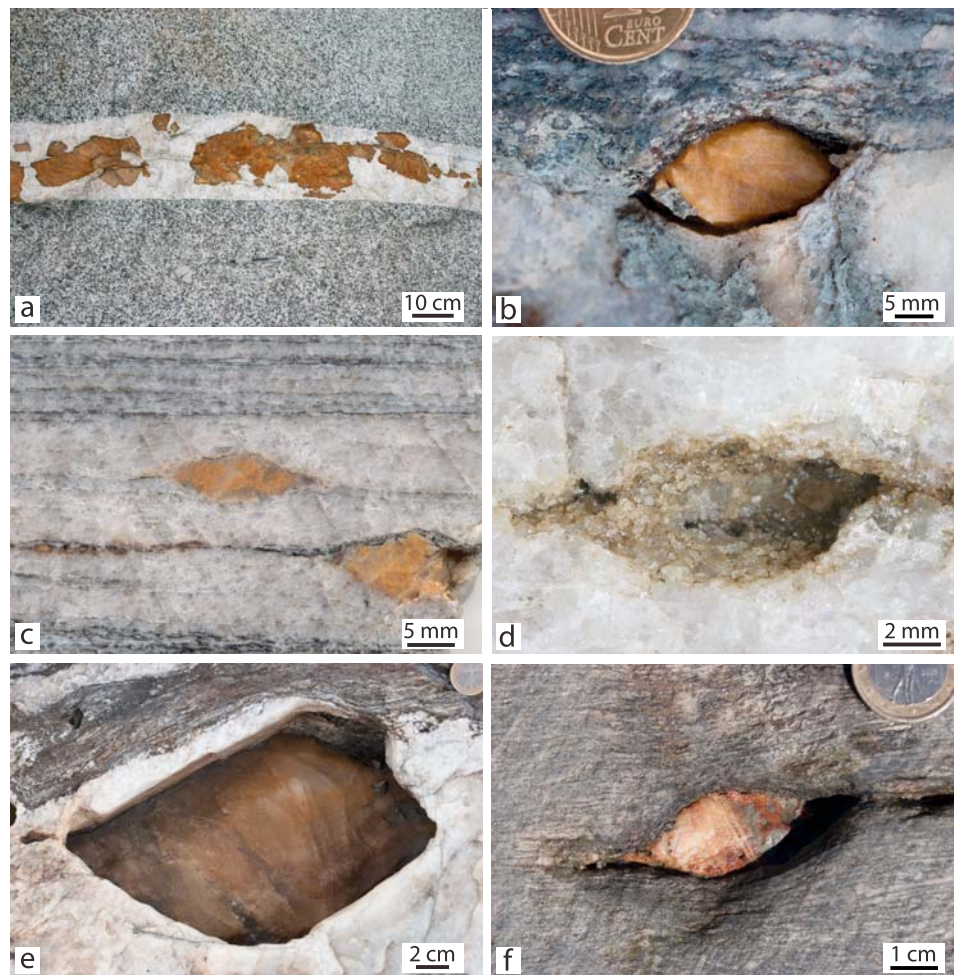


Figure 1. (a) Undeformed vein within granodiorite filled with quartz (white) and large crystals of calcite (dark). Looking down, top to east. (b) Single-crystal calcite porphyroclast at the boundary between mylonitic vein quartz (below) and sheared granodiorite (above). The long axis of the clast is oblique to the foliation, consistent with a dextral shear sense. Looking down, top to north. (c) Polished surface of mylonitic vein quartz including calcite porphyroclasts. (d) Negative shape of a calcite porphyroclast that has weathered out of a mylonitic vein quartz matrix, showing the positive relief of quartz grains against the original calcite. (e) Large single-crystal calcite clast in a dextrally sheared quartz vein. Note the characteristic asymmetric shape, consistent with the dextral sense, and the clear evidence against rolling of the clast provided by the only slightly bowed boundary of the quartz vein against the surrounding biotite-rich sheared granodiorite. Looking down, top to north. (f) Single-crystal calcite porphyroclast in a granodiorite mylonite. Sense of shear dextral, view looking down, top to north. The surface of observation in all cases is approximately perpendicular to foliation and parallel to lineation (XZ).

of twins was obtained over temperatures in the range 200°C–800°C, which is appropriate to the deformation conditions in Neves. However, the aim of their study was obviously to calibrate twinning incidence, twin density and volume percent twinning (see the original paper of *Rowe and Rutter* [1990] for a definition of these terms) against differential stress for a range of grain sizes, rather than establishing any lower stress cutoff to the appearance of twins. Their lowest stress experiment (KTM8, in *Rowe and Rutter's* Table 1), with 39 MPa at 10% strain, still has a maximum of 9 vol. % of twins for the 800 μm grain size. Since we see no evidence of high-temperature twinning, the inference is that flow stress during amphibolite facies shearing in the Neves area was significantly less than 39 MPa.

[15] The size of subgrains and dynamically recrystallized new grains in the calcite clasts also provides an estimate of the differential stress at the time of their formation, and experimental calibrations for Carrara marble have been provided by *Schmid et al.* [1980] and *Rutter* [1995]. Unfortunately, the millimeter-scale size of subgrains and, where developed, new grains, is outside their calibration range [e.g., *Rutter*, 1995, Figure 7]. However, what is clear is that the magnitude of the differential stress must be <10 MPa. Similarly, the surrounding quartz mylonite matrix has dynamically recrystallized by a grain boundary migration mechanism, also with grain sizes on the millimeter scale, and this microstructure was not later modified by annealing or grain growth (Figure 2b). This grain size is

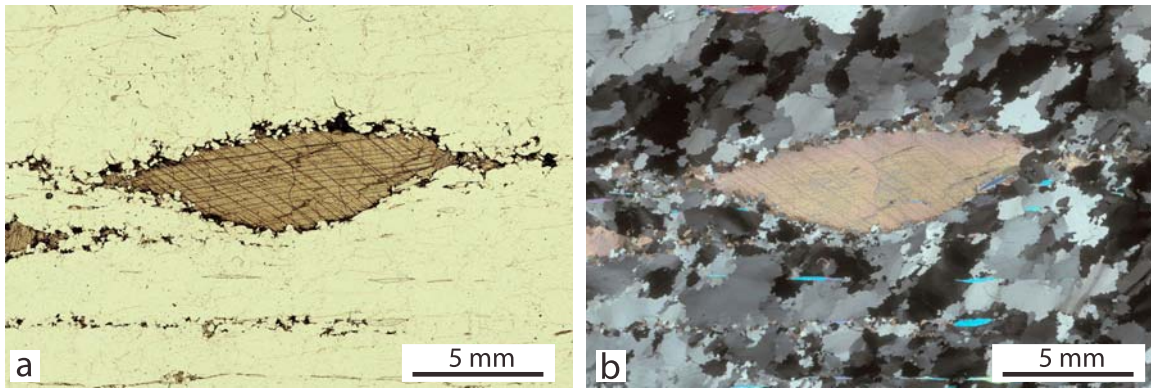


Figure 2. (a) Photomicrograph in plane light of vein quartz mylonite with single-crystal calcite porphyroclast. Note the indentation of quartz grains into the calcite single-crystal, the lack of recrystallization or evidence of crystal plastic deformation in the calcite and the two sets of (late) twins. (b) Same view under crossed polars. Note the coarse-grained dynamically recrystallized quartz microstructure with irregular lobate grains typical of deformation under amphibolite facies conditions. The oblique shape fabric is consistent with a dextral shear sense. In both cases, the surface of observation is perpendicular to foliation and parallel to lineation (XZ).

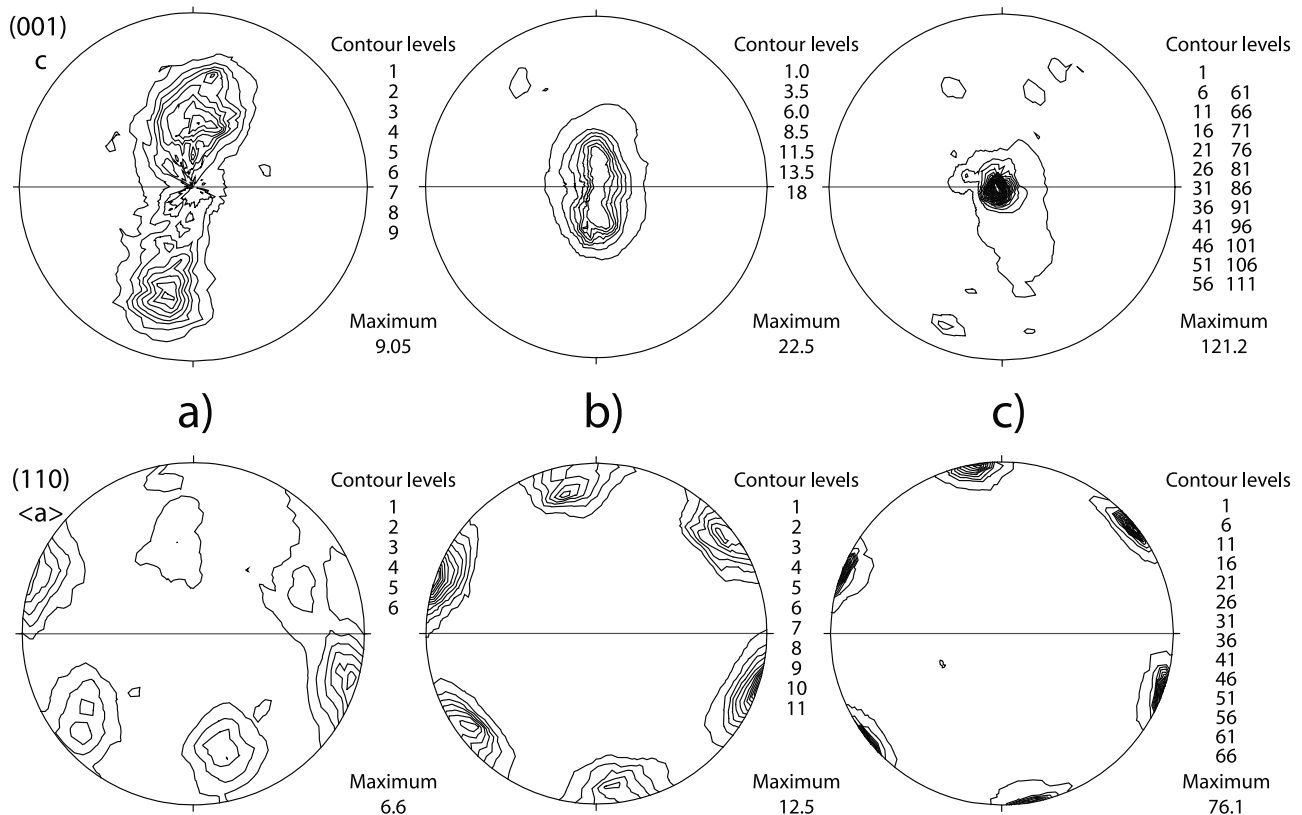
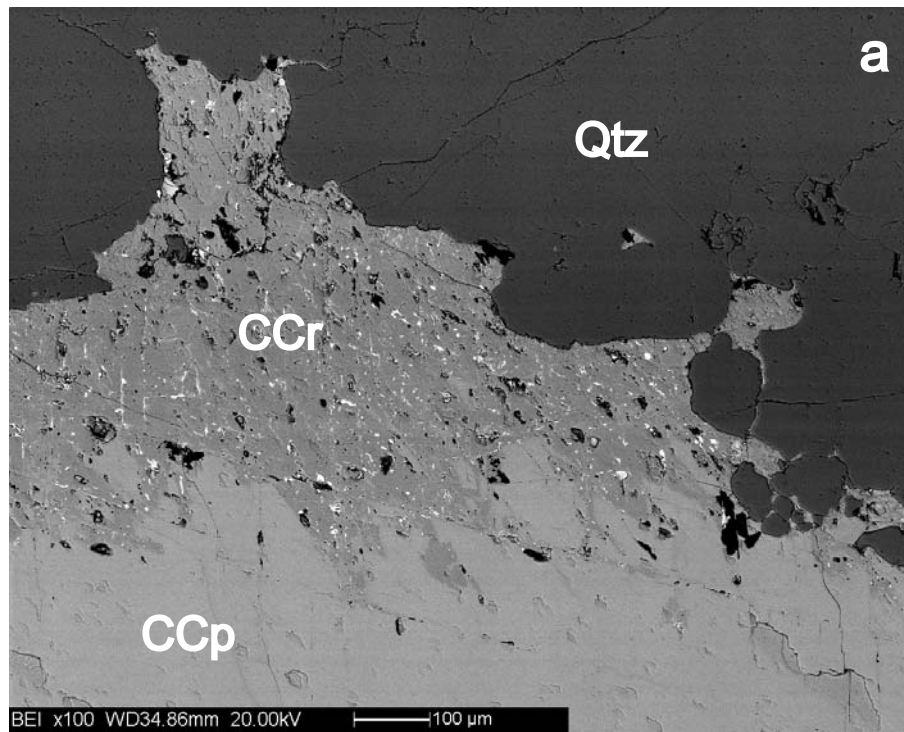


Figure 3. CPO, measured by X-ray texture goniometry, of 3 different quartz mylonites that contain calcite porphyroclasts. The upper row is for the c axis (001) and the lower row for the prism $\langle a \rangle$ (110). (a) A combined plot of 4 spot analyses of the sample shown in Figure 1c, corresponding to a total investigated area of $\sim 4 \text{ cm}^2$. (b and c) Single scans ($\sim 1 \text{ cm}^2$ each) from the quartz mylonite matrix surrounding isolated calcite porphyroclasts but sufficiently removed that perturbations in flow due to the clast itself are avoided. Plots are equal-area upper hemisphere stereographic projections, with the foliation oriented E-W and vertical (as indicated by the gray line), the lineation horizontal and the sense of shear dextral.



| | PORPHYROCLAST | | | | | | | | | | | | |
|-----------------|---------------|--------|-------|-------|-------|--------|--------|--------|--------|--------|-------|-------|------|
| | 1 | 2 | 3 | 4 | 5 | 6 | 7 | 8 | 9 | 10 | 11 | mean | s.d. |
| MgO | 0.39 | 0.45 | 0.45 | 0.49 | 0.46 | 0.56 | 0.48 | 0.41 | 0.36 | 0.50 | 0.26 | 0.44 | 0.08 |
| CaO | 53.16 | 52.92 | 52.43 | 52.08 | 52.56 | 52.65 | 52.79 | 53.04 | 53.22 | 52.79 | 52.77 | 52.76 | 0.33 |
| MnO | 0.53 | 0.53 | 0.71 | 0.62 | 0.45 | 0.70 | 0.46 | 0.70 | 0.53 | 0.65 | 0.49 | 0.58 | 0.10 |
| FeO | 2.32 | 2.33 | 2.40 | 2.58 | 2.49 | 2.31 | 2.50 | 2.08 | 2.12 | 2.78 | 2.49 | 2.40 | 0.20 |
| CO ₂ | 43.89 | 43.77 | 43.55 | 43.37 | 43.56 | 43.78 | 43.77 | 43.77 | 43.78 | 44.08 | 43.52 | | |
| Total | 100.29 | 100.00 | 99.55 | 99.14 | 99.52 | 100.00 | 100.00 | 100.00 | 100.00 | 100.80 | 99.52 | | |

| | RIM | | | | | | | | | | | | | | | |
|-----------------|-------|--------|--------|-------|-------|--------|--------|--------|--------|--------|--------|--------|--------|--------|-------|------|
| | 1 | 2 | 3 | 4 | 5 | 6 | 7 | 8 | 9 | 10 | 11 | 12 | 13 | 14 | mean | s.d. |
| MgO | 0.08 | 0.00 | 0.08 | 0.02 | 0.00 | 0.00 | 0.02 | 0.43 | 0.35 | 0.30 | 0.08 | 0.09 | 0.06 | 0.00 | 0.11 | 0.14 |
| CaO | 55.13 | 55.73 | 55.61 | 55.74 | 55.68 | 56.37 | 56.26 | 55.63 | 55.68 | 56.08 | 55.52 | 55.85 | 55.93 | 56.32 | 55.82 | 0.34 |
| MnO | 0.26 | 0.05 | 0.10 | 0.06 | 0.05 | 0.04 | 0.00 | 0.09 | 0.09 | 0.00 | 0.03 | 0.00 | 0.12 | 0.00 | 0.06 | 0.07 |
| FeO | 0.27 | 0.28 | 0.26 | 0.11 | 0.06 | 0.12 | 0.11 | 0.23 | 0.32 | 0.07 | 0.55 | 0.07 | 0.12 | 0.09 | 0.19 | 0.14 |
| CO ₂ | 43.68 | 43.94 | 43.95 | 43.87 | 43.76 | 44.34 | 44.25 | 44.33 | 44.33 | 44.38 | 44.02 | 43.98 | 44.10 | 44.25 | | |
| Total | 99.41 | 100.00 | 100.00 | 99.81 | 99.54 | 100.87 | 100.64 | 100.72 | 100.76 | 100.83 | 100.22 | 100.00 | 100.33 | 100.65 | | |

Figure 4. (a) Scanning electron microscope backscattered image of the border of a calcite porphyroblast (CCp, light gray) showing a rim of almost pure calcite (CCr, darker gray) disseminated with Mn-Fe-rich grains (bright) in contact with quartz (Qtz, dark gray to black). Note the irregular calcite-quartz boundary. (b) Mean compositions of calcite porphyroclasts and rims obtained with a Cameca SX 50 (working conditions are accelerating voltage 20 kV, beam current 10 nA).

again beyond the experimentally calibrated range for flow stress versus recrystallized grain size in quartz [Stipp and Tullis, 2003; Stipp *et al.*, 2006], but once more the flow stress must be <10 MPa.

[16] This rather low differential stress was sufficient for quartz to flow and develop a quartz mylonite, whereas the single-crystal calcite grains remained effectively rigid. In the field, it can be demonstrated that localized shearing occurred even on quartz veins that were oriented almost orthogonal to the direction of bulk shortening, for which the

resolved shear stress must have been very low [Pennacchioni and Mancktelow, 2007]. This implies that the polycrystalline quartz in these veins had (1) a viscous rheology, without any significant yield strength, and (2) a low effective viscosity, consistent with the predicted flow stress of <10 MPa.

4. Rheology of Calcite and Quartz

[17] The published literature on experimentally determined quartz and calcite rheology and on the extrapolation

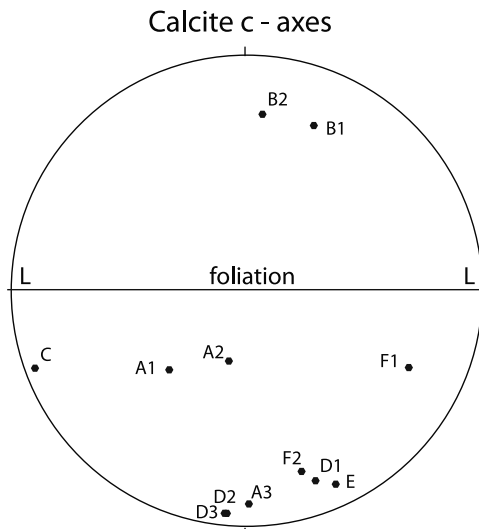


Figure 5. Equal-area upper hemisphere projection of the c axis orientation of six calcite porphyroclasts (A–F) measured by X-ray texture goniometer. Measurements of different grains or twin domains in single clasts are indicated by numbers (e.g., A1, A2, A3). Foliation oriented E–W and vertical, lineation approximately horizontal (lineation in some cases only approximately determinate, to within $\sim 5^\circ$).

of these results to natural conditions is extensive. Figure 7 summarizes the results for wet quartzite compared to calcite single crystals and coarse grained calcite marbles. For simplicity, the (extrapolated) curves are those from the original publications, as determined under axial compression. As discussed further below, a correction should be applied if the deformation geometry is different and, in particular, if it is one of simple shear rather than axial compression. Also indicated on Figure 7 are the range in strain rates obtained under experimental conditions and a possible range of natural conditions in the Neves area. The “broad” rectangle limits the interpreted range in strain rate, from $3 \times 10^{-11} \text{ s}^{-1}$ (i.e., a shear strain $\gamma \sim 1000$ in 1 Ma) to $3 \times 10^{-15} \text{ s}^{-1}$ (i.e., a shear strain $\gamma \sim 1$ in 10 Ma) and

differential stress $< 30 \text{ MPa}$. The maximum strain rate in this range corresponds to values of $10^{-10} - 10^{-11} \text{ s}^{-1}$ estimated by *Herwegh et al.* [2005] for narrow ($< 20 \text{ m}$) thrust zones in the Helvetic Alps, which have displacements of ca. 25 km. Considering that the Neves area is a generally low strain domain [*Pennacchioni and Mancktelow, 2007*], the realistic range in strain rate in the Neves area is likely to be considerably smaller, with a “narrow” range indicated for strain rates from $3 \times 10^{-12} \text{ s}^{-1}$ to $3 \times 10^{-14} \text{ s}^{-1}$ and, as discussed above, a differential stress interpreted to be $< 10 \text{ MPa}$. It may be noted that the minimum strain rate is the same as the minimum strain rate of 3 to $4 \times 10^{-14} \text{ s}^{-1}$ recently estimated in some natural ductile shear zones by *Sassier et al.* [2009].

[18] It is immediately obvious from Figure 7 that, even without plotting the corresponding error ranges on the extrapolated experimental curves, there is a significant scatter in the results, in part reflecting the major extrapolation involved in going from experimental to natural conditions. However, it is also clear that, in general, coarse calcite shows a weaker strain rate sensitivity than quartzite. As a result, there is a tendency for the bundle of calcite curves to intercept the bundle of quartzite curves with decreasing strain rate and, therefore, the potential for coarse calcite to be stronger than wet quartzite at natural (low) strain rates.

[19] At laboratory strain rates, calcite single crystals and coarse marbles deformed at relatively low laboratory temperatures ($< 700^\circ\text{C}$) show very low strain rate sensitivity. The data can be approximated either by a power law relationship with a high n value (e.g., $n \approx 13$ for the 600°C data of *de Bresser and Spiers* [1990]) or by an exponential relationship [*Rutter, 1974; Schmid et al., 1980; de Bresser and Spiers, 1990, Table 3*]. At higher temperature and lower stress, calcite deforming by dislocation creep shows a general power law relationship between strain rate and stress ($\dot{\epsilon} \propto \sigma^n$), with a stress exponent n that decreases both with decreasing grain size and increasing temperature (and therefore decreasing flow stress). However, for coarse grain sizes (single crystals and marbles with grain size $> 100 \mu\text{m}$), n values are still significantly higher than the

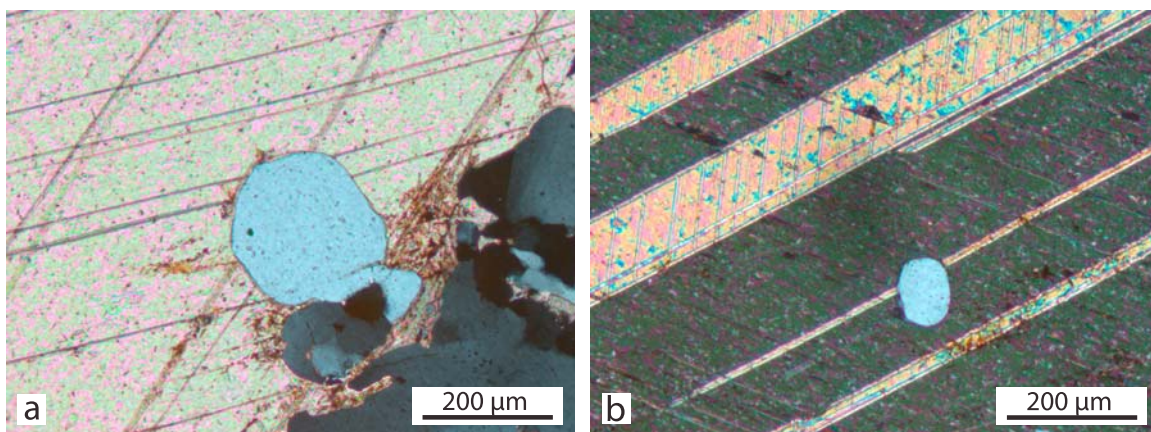


Figure 6. Photomicrographs under crossed polars of calcite porphyroclasts from near the rim, where small quartz inclusions crosscut straight twins. Note that both (a) relatively thin and (b) coarse twins can be developed, often in the same calcite crystal (Figure 6b) and that there is no evidence for bulging or recrystallization along twin boundaries.

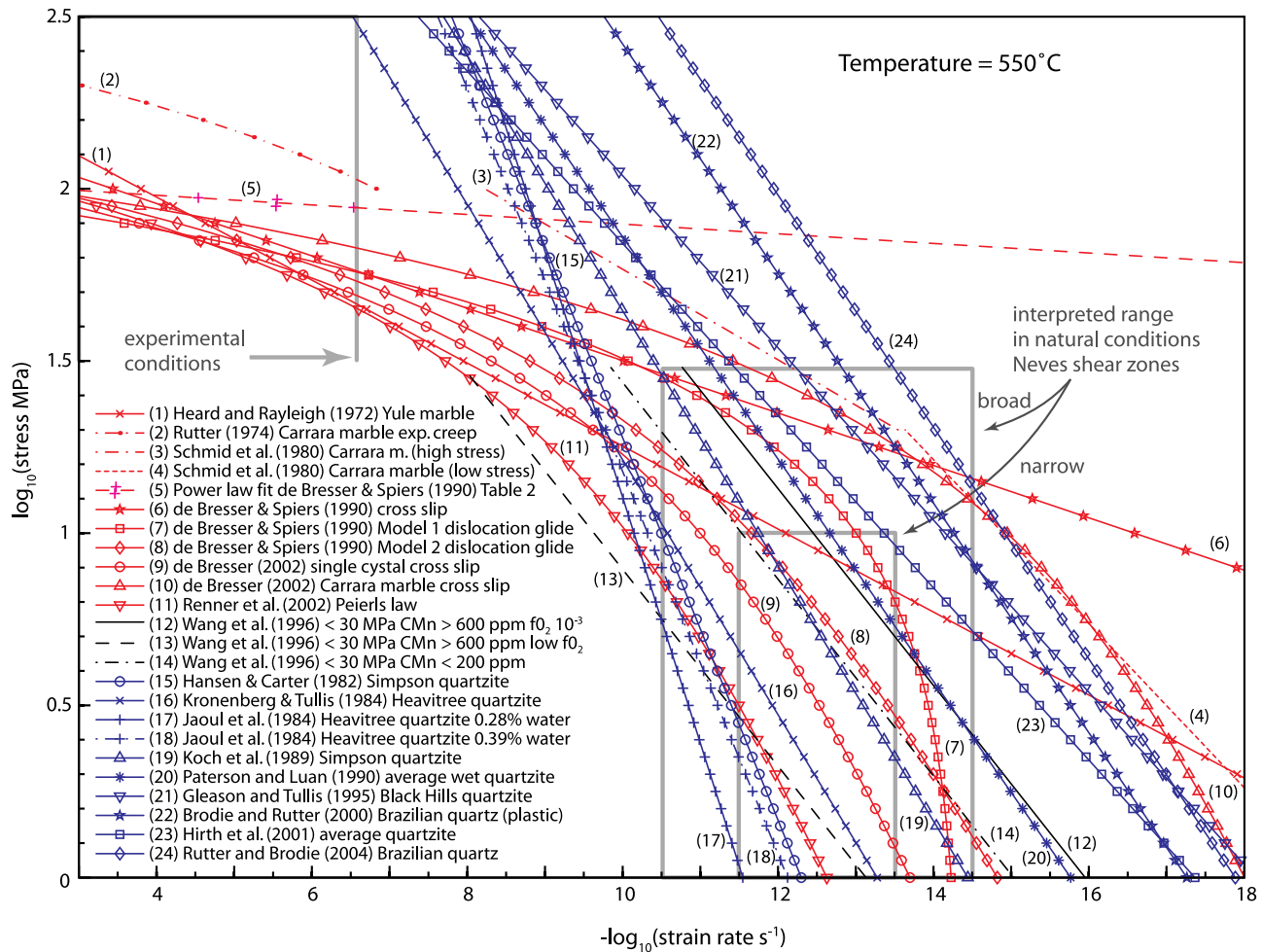


Figure 7. Extrapolation of selected experimental data for creep of single calcite crystals [*de Bresser and Spiers*, 1990; *de Bresser*, 2002; *Wang et al.*, 1996], coarse-grained marble [*Heard and Raleigh*, 1972; *Rutter*, 1974; *Schmid et al.*, 1980] and synthetic polycrystalline calcite [*Renner et al.*, 2002] and natural and synthetic “wet” quartzite [*Hansen and Carter*, 1982; *Jaoul et al.*, 1984; *Kronenberg and Tullis*, 1984; *Koch et al.*, 1989; *Paterson and Luan*, 1990; *Gleason and Tullis*, 1995; *Brodie and Rutter*, 2000; *Hirth et al.*, 2001; *Rutter and Brodie*, 2004b] to possible geological strain rates at 550°C. The original authors emphasized that some results are only appropriate for a specific range: curve 2 above 100 MPa, curve 3 in the range 20–100 MPa, curve 4 for <20 MPa, and curves 12, 13, and 14 for <30 MPa. Calculation of curve 11 from *Renner et al.* [2002] used the parameters listed in their abstract for a grain size of 1 cm, the order of magnitude for the calcite porphyroclasts. The extrapolations of *Hirth et al.* [2001] and *Rutter and Brodie* [2004b] involve a linear dependence of strain rate on water fugacity. For the figure, a water pressure of 500 MPa is assumed and, from Table 8 of *Tödheide* [1972], a fugacity coefficient at 550°C of 0.506. The “broad” rectangle limits the interpreted extreme range in strain rate, from $3 \times 10^{-11} \text{ s}^{-1}$ to $3 \times 10^{-15} \text{ s}^{-1}$ and differential stress <30 MPa that could be possible in the Neves area. A more likely “narrow” range restricts the conditions to $3 \times 10^{-12} \text{ s}^{-1}$ to $3 \times 10^{-14} \text{ s}^{-1}$ and differential stress <10 MPa. For simplicity in extrapolation, the plot is for uniaxial shortening, which is the geometry employed in the experiments.

value of ~ 3 generally predicted for climb-controlled dislocation creep [*Poirier*, 1985; *Weertman*, 1955, 1968]. In the experiments of *de Bresser and Spiers* [1990], n decreases from 72 ± 37 at 550°C to 9.6 ± 0.6 at 800°C, whereas for the experiments on Carrara marble by *Schmid et al.* [1980], n decreases from 14 ± 0.1 at 600°C to 4.4 ± 0.5 at 1050°C. These results are summarized in Figures 1 and 3 of *de Bresser* [2002], who emphasized the clear decrease in n with increasing temperature and who proposed that cross-slip controlled by the dissociation of dislocations offered the

best explanation for the observed mechanical behavior. New axial shortening experiments by *de Bresser* [2002] again confirmed the low strain rate sensitivity of flow stress, with single crystals deformed at $T = 800^\circ\text{C}$ and strain rate $\sim 10^{-5} \text{ s}^{-1}$ having $n = 10.3 \pm 0.1$ and Carrara marble $n \sim 12$ at 800°C, $n \sim 9$ at 900°C and $n \sim 5$ at 1000°C. *de Bresser* [2002] compared the experimental data with models for climb-controlled creep and cross-slip-controlled creep, with either constriction before cross slip or dissociation afterward controlling creep. He “tentatively

concluded that the dissociation controlled cross-slip model offers the best description of dislocation creep behavior of calcite at intermediate conditions.” This model has also been used to extrapolate laboratory data to nature in the more recent study of *Herwegh et al.* [2005]. *Pieri et al.* [2001] reported that, for Carrara marble with an initial grain size of 150 μm deforming in torsion within the dislocation creep regime, the stress exponent was ~ 10 and decreased only slowly to ~ 6 for shear strain $\gamma = 9$ (at 1000 K, i.e., $\sim 730^\circ\text{C}$) or not at all (at 1200 K, $\sim 930^\circ\text{C}$). This was despite the fact that at this strain the marble was almost completely recrystallized to a fine grain size of about 10 μm (1000 K) or 20 μm (1200 K).

[20] The calcite from Neves contains minor amounts of Fe, Mn, and Mg. The laboratory results of *Wang et al.* [1996] (Figure 7) are therefore of specific interest, because they considered the effect of Mn impurity on calcite rheology for a large range of oxygen fugacities. Similar to previous studies [e.g., *Schmid et al.*, 1980; *de Bresser and Spiers*, 1990; *de Bresser*, 2002] they observed a difference in the effective power law stress exponent for different stress regimes, with the low-stress regime (<30 MPa) having $n \sim 3.5 \pm 0.5$ and the high-stress regime $n \sim 6-15$. In the high-stress regime, n apparently increases with stress, indicating power law creep breakdown. In the low-stress regime (as appropriate to the Neves area) and for normal oxygen fugacities ($f_{\text{O}_2} < 10^{-8}$ bar), their results indicate that samples with high Mn concentrations (>600 ppm, curve 13 on Figure 7) should be substantially weaker than those with low Mn (<200 ppm, curve 14). The relatively high Mn content of the Neves calcite should not therefore be the cause of its strong behavior relative to quartz. The Neves calcite also contains significant amounts of Fe and Mg, but there are no published studies considering possible effects of these impurities on dislocation creep in coarse calcite (>100 μm). The field observations of *Delle Piane et al.* [2008] suggest that calcite can be stronger than dolomite under upper amphibolite facies conditions. The results of their laboratory deformation experiments with fine grained (~ 5 μm) hot-pressed dolomite powder are consistent with these field observations. However, more recently, the study of *Xu et al.* [2009] on high-magnesian calcite with a grain size in the range 8–31 μm suggests the opposite influence of Mg in calcite: for a given strain rate, constant temperature and fixed grain size, the strength of calcite in the dislocation creep regime increased with Mg solute content. This would imply that Mn and Mg impurities have opposite effects, with Mn weakening and Mg strengthening calcite. It should also be noted that Mn and Mg have opposite effects on the normal grain growth of calcite, with Mn increasing [*Freund et al.*, 2001] and Mg decreasing [*Herwegh et al.*, 2003] growth rates. Experiments on the effect of Fe on the deformation of calcite in the dislocation creep regime are still lacking.

[21] The rheology of quartz deforming by dislocation creep has generally been described in terms of a power law relationship:

$$\dot{\epsilon} = A f_{\text{H}_2\text{O}}^m e^{(-Q/RT)} \sigma^n$$

with experimentally determined n values ranging from 1.4 to 1.8 [*Jaoul et al.*, 1984], to ~ 3 [*Kronenberg and Tullis*,

1984; *Koch et al.*, 1989; *Paterson and Luan*, 1990; *Rutter and Brodie*, 2004b], to ~ 4 [*Gleason and Tullis*, 1995; *Hirth et al.*, 2001]. Recent studies generally argue that the appropriate n value should lie in the range 3–4 [*Hirth et al.*, 2001; *Rutter and Brodie*, 2004b]. *Paterson and Luan* [1990] and *Hirth et al.* [2001] both propose the activation energy Q to be ~ 135 kJ mol^{-1} , which is practically identical to the activation energy for silicon bulk diffusion in novaculite under hydrothermal conditions determined experimentally by *Farver and Yund* [2000] ($Q = 137 \pm 18$ kJ mol^{-1}). However, other experimental studies on dislocation creep in wet quartzites have returned rather higher values, in the range $Q \sim 220-240$ kJ mol^{-1} [*Gleason and Tullis*, 1995; *Brodie and Rutter*, 2000; *Rutter and Brodie*, 2004a, 2004b]. The effect of water fugacity $f_{\text{H}_2\text{O}}$ is not well established but most studies have concluded that the dependence is close to direct proportionality with $m \sim 1$ [*Gleason and Tullis*, 1995; *Hirth et al.*, 2001; *Rutter and Brodie*, 2004b] to $m \sim 1.2$ [*Kohlstedt et al.*, 1995]. *Farver and Yund* [1991] also established a linear correlation with $f_{\text{H}_2\text{O}}$ for the self diffusion rate of oxygen in quartz. However, the experimental work of *Post et al.* [1996] suggests a stronger power law dependence, with $m > 2$, whereas the most recent work of *Chernak et al.* [2009] suggests that $0.375 \leq m \leq 1$ (assuming $n \sim 3-4$). The water fugacity is related to the water pressure via the fugacity coefficient, values of which were interpolated from Table 8 of *Tödheide* [1972], assuming a pressure of 500 MPa, which is in the midrange of values for the water-rich fluid pressure estimated by *Cesare et al.* [2001] for the Neves area.

[22] The laboratory results discussed above and extrapolated to natural conditions in Figure 7 were conducted under axial compression. However, the natural examples considered here certainly developed in effectively plane strain shear zones under conditions approaching simple shear. Transformation of power law rheology from axial shortening to simple shear reduces the effective viscosity by a factor $2^{1/n} 3^{-(1+1/n)/2}$ [e.g., *Ranalli*, 1987; *Schmid et al.*, 1987; *Johnson and Fletcher*, 1994], from which it follows that the ratio of the shear stress τ_{xy} in simple shear to the differential stress $\Delta\sigma = (\sigma_1 - \sigma_2)$ in axial shortening is $3^{-(1+1/n)/2}$. Therefore, for the same “strain rate,” it can be shown that (1) the flow stress is lower in simple shear by a factor that varies from 1/3 for linear viscous materials to ~ 0.57 for large stress exponents n and (2) the viscosity contrast with markedly different n values will be increased, although the increase cannot exceed ~ 2 and will generally be considerably less.

[23] From Figure 7 it is seen that there is rather a wide range of extrapolated curves that could be considered when considering the relative strength of coarse calcite and wet quartzite under conditions appropriate to the Neves area. However, some combinations would not result in the observation that calcite can be significantly stronger than quartz. In particular, curve 11 of *Renner et al.* [2002] using a Peierls law approach would predict that calcite is always weaker or of similar strength to quartz. *de Bresser and Spiers* [1990], *de Bresser* [2002] and *Herwegh et al.* [2005] have argued that cross slip is the dominant mechanism controlling crystal plastic deformation of coarse calcite, with the corresponding curves 6, 9, and 10 on Figure 7. Of these, curves 6 and 10 are the most likely to result in an

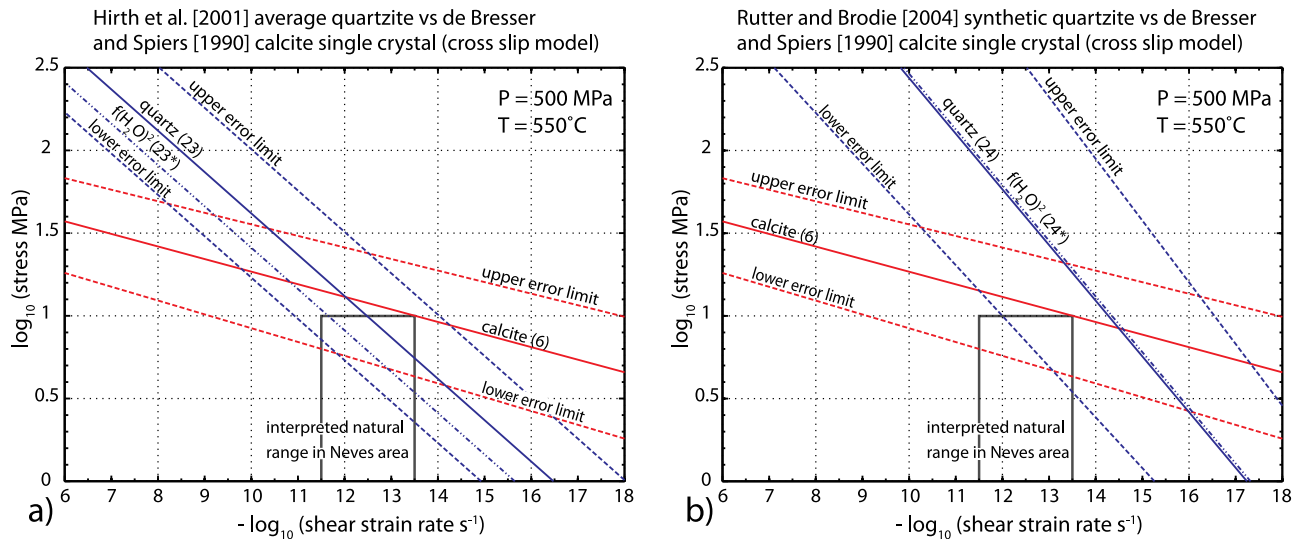


Figure 8. Plots of the effect of the reported errors in determined experimental flow laws for calcite and quartz and the possible influence of differing dependence on water fugacity. Calcite (curve 6 from Figure 7) corresponds to the model of dislocation creep controlled by cross slip presented by *de Bresser and Spiers* [1990] and is plotted in both Figures 8a and 8b. (a) Quartz (curve 23 from Figure 7) is the model for average quartzite of *Hirth et al.* [2001], with a linear dependence on water fugacity and “ $f(\text{H}_2\text{O})^2$ (23*)” is the same model assuming a quadratic dependence on water fugacity. (b) Quartz (24 from Figure 7) and “ $f(\text{H}_2\text{O})^2$ (24*)” are the corresponding plots for the experimentally derived model of *Rutter and Brodie* [2004b]. The “narrow” range of potential natural conditions at Neves is also indicated, consistent with Figure 7. The fugacity coefficient of water is calculated in each case by interpolating from Table 8 of *Tödheide* [1972]. The extrapolations are corrected for a simple shear flow, following *Johnson and Fletcher* [1994].

inversion in strength of calcite relative to quartz with decreasing strain rate. Curve 6 is effectively a power law relation, with n varying as a function of temperature, and therefore plots as a straight line on the log-log plot of Figure 7. Such a power law relationship has the advantage that it can be readily transformed from axial shortening to simple shear as outlined above. For simplicity, it is therefore relationship curve 6 that is used below to compare coarse calcite with wet quartzite under conditions appropriate to the natural shear zones of the Neves area.

[24] Figure 8 presents this comparison with the average quartzite of *Hirth et al.* [2001] (curve 23) and the synthetic quartzite of *Rutter and Brodie* [2004b] (curve 24). These were chosen because they give error ranges for their estimated parameters and include a dependence on water fugacity. The influence of water may be of paramount importance, because it is now well established that water has a dramatic influence on dislocation creep in quartz [*Griggs and Blacic*, 1965; *Griggs*, 1967; *Paterson*, 1989; *Tullis and Yund*, 1989] but effectively none on calcite [*Rutter*, 1974; *de Bresser et al.*, 2005]. If error ranges are included, extrapolation of both quartzite flow laws would intersect the interpreted natural range of conditions for the Neves area, although the overlap is clearly greater in Figure 8a [i.e., *Hirth et al.*, 2001]. If error ranges are not considered, the combination of the *Rutter and Brodie* [2004b] quartzite with the *de Bresser and Spiers* [1990] model for cross-slip control in single-crystal calcite would not result in a relative inversion in strength of coarse calcite to quartz at realistic natural strain rates.

[25] Both flow laws for quartzite include a linear dependence on water fugacity. However, the study of *Post et al.* [1996] suggested a quadratic dependence, and the potential effect of such a relationship is also explored in Figure 8. The published flow laws were recast for the proposed water fugacity of 37 MPa in the Ruby Gap duplex natural example of *Hirth et al.* [2001] and for the 300 MPa water fugacity in the experiments of *Rutter and Brodie* [2004b]. They were then extrapolated to 500 MPa water pressure and 550°C, conditions considered appropriate to the Neves area, with the fugacity coefficient interpolated from Table 8 of *Tödheide* [1972]. Rather surprisingly, the effect of quadratic water fugacity dependence is not that dramatic for these examples. It does result in somewhat lower predicted flow stress for quartz in Figure 8a but has almost no effect in Figure 8b, because, relative to the experimental conditions of *Rutter and Brodie* [2004b], the influence of higher water pressure is counteracted by that of lower temperature.

[26] Figure 9 shows the effective viscosity ratio between calcite and quartz for simple shear over a range of temperature and strain rate conditions. The same cross-slip-controlled flow law for calcite single crystals is used as in Figure 8 [*de Bresser and Spiers*, 1990] and in Figure 9a the quartz flow law is also the same as Figure 8a [i.e., *Hirth et al.*, 2001]. For this combination, the maximum effective viscosity ratio for coarse calcite relative to quartzite is ≤ 2 for geological strain rates $\geq 10^{-14} \text{ s}^{-1}$. As noted above, if the combination presented in Figure 8b was used, calcite would always be weaker than quartz. In Figure 9b, the comparison is made with the results for Heavitree quartzite of *Kronenberg*

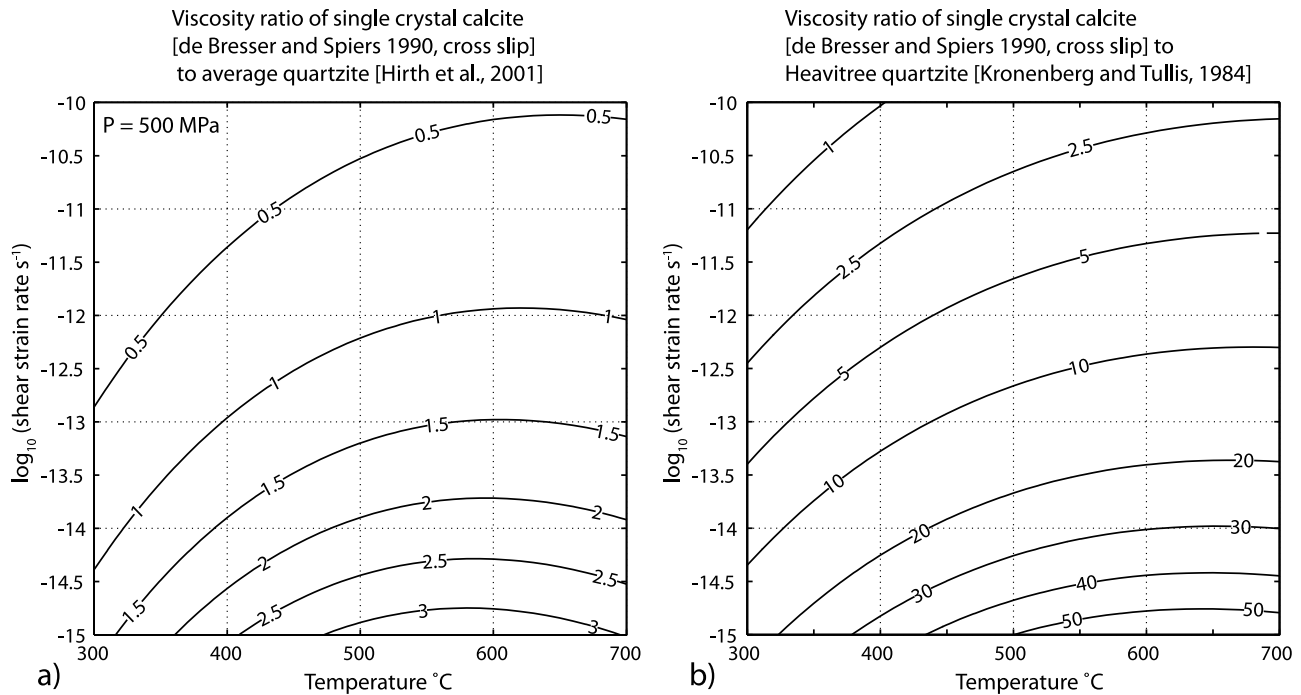


Figure 9. Calculated viscosity ratios for single-crystal calcite following the cross-slip-controlled dislocation creep model of *de Bresser and Spiers* [1990] relative to (a) average quartzite of *Hirth et al.* [2001] and (b) Heavittree quartzite with 0.4% water added of *Kronenberg and Tullis* [1984], as tabulated in Table 3c of *Evans and Kohlstedt* [1995]. In Figure 9a, a water pressure of 500 MPa is assumed and the water fugacity coefficient determined by polynomial interpolation from Table 8 of *Tödheide* [1972]. Extrapolations of the laboratory data, based on axial compression, are corrected for a simple shear flow, following *Johnson and Fletcher* [1994].

and *Tullis* [1984] that are tabulated in Table 3c of *Evans and Kohlstedt* [1995]. This is presented as an example of a combination that would predict a rather higher range of viscosity ratios. However, even in this case, the maximum effective viscosity ratio of coarse calcite to quartzite is still ≤ 30 for geological strain rates $\geq 10^{-14} \text{ s}^{-1}$.

5. Numerical Modeling

[27] As established above, coarse or single-grain calcite may be stronger than wet quartzite for the midcrustal conditions and range of strain rates appropriate to shear zone development in the Neves area. However, the predicted effective viscosity ratios are not particularly large (Figure 9). For linear viscous behavior in two dimensions, a particle with an initially circular cross section and viscosity 10 times the viscosity of the surrounding matrix should elongate at a rate ~ 5 times slower than the same circular clast without any viscosity contrast [*Mulchrone and Walsh*, 2006, equation (3)]. The shear strain γ in the shear zones containing the calcite porphyroclasts is large, as is reflected, for example, in the extreme elongation of original biotite clots in the granodiorite protolith. The practically undeformed calcite porphyroclasts would therefore require unrealistically high viscosity ratios if the materials behaved in a linear viscous manner. However, as discussed above, neither calcite nor quartzite is expected to be linear viscous for the grain sizes and natural conditions involved. Rather

they should show a power law behavior, with a stress exponent for quartzite of around 3–4 and for calcite rather higher (generally ≥ 6), although the stress exponent for calcite decreases with increasing temperature and/or flow stress (for similar coarse grain size).

[28] The influence of power law rheology on the behavior of an isolated inclusion within a homogeneous, isotropic matrix deforming in simple shear was therefore investigated in a series of finite element models, using a personally developed code [*Mancktelow*, 2006, 2008]. Incompressible power law viscous flow is assumed, with a coherent interface between particle and matrix. Figure 10 presents the results for the shape of an initial circular particle after a shear strain of $\gamma = 6$, for different effective viscosity ratios and power law exponents. The effective viscosity ratio is defined as that for equal strain rate inside and outside the particle. Such a uniform strain rate distribution is assumed at run initiation, but iteration toward convergence in the very first time step soon establishes a realistic distribution. Following remeshing steps, carried out automatically when mesh distortion becomes excessive, the strain rate is interpolated to new nodal positions, so that this assumption need only be made once at the beginning of any numerical model.

[29] If both inclusion and matrix have a linear viscosity, the stress (and thus strain rate and strain) is uniform within the particle [*Eshelby*, 1957; *Schmid and Podladchikov*, 2003] and the particle maintains an elliptical shape during

Inclusion Shape for $\gamma = 6$ in Dextral Simple Shear

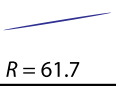
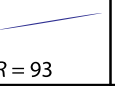
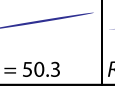
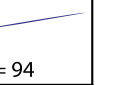



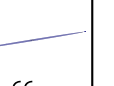



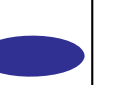
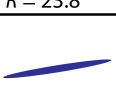
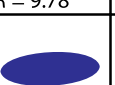


| $\frac{n_i}{n_m} \backslash \frac{\mu_i}{\mu_m}$ | 1 / 1 | 3 / 3 | 3 / 1 | 6 / 3 |
|--|---|---|---|---|
| 1 / 2 |  $R = 61.7$ |  $R = 93$ |  $R = 50.3$ |  $R = 94$ |
| 1 / 1.5 |  $R = 52.2$ |  $R = 72$ |  $R = 34.7$ |  $R = 66$ |
| 1.5 / 1 |  $R = 23.8$ |  $R = 9.78$ |  $R = 2.99$ |  $R = 2.58$ |
| 2 / 1 |  $R = 15.4$ |  $R = 2.95$ |  $R = 1.50$ |  $R = 1.13$ |

Figure 10. Shape of an isolated cylindrical inclusion, with an initially circular cross section, for incompressible 2-D dextral simple shear flow to a background shear strain value of $\gamma = 6$. Both inclusion and matrix have a power law (or linear viscous) rheology. Values of the stress exponent for inclusion (n_i) and matrix (n_m) are given along the top and values of the effective viscosity ratio (μ_i/μ_m) down the left (for the case of equal strain rate in inclusion and matrix). The axial ratio R of the inclusion at $\gamma = 6$ is also given, estimated using a simplex least squares routine to determine a best fit ellipse for nodal points on the periphery of the inclusion. Values of R for weak inclusions in a power law matrix are only given to two significant digits, reflecting the fact that their deformed shape is not strictly elliptical. For reference, $R = 37.97$ at $\gamma = 6$ for a passive inclusion (“strain ellipse”). Note that the inclusion plots are not at the same scale but have been modified to fit in the space available.

deformation. The current numerical modeling shows that this is still the case for power law viscous inclusions embedded in a linear viscous matrix, but not if the matrix itself is nonlinear. The final inclusion shape when the matrix is nonlinear is only approximately elliptical, although the difference is not significant except for strongly elongate particles (as implied in Figure 10 for those examples where the axial ratio R to the best fit ellipse is only given to two significant digits).

[30] As can be seen from Figure 10, power law rheology has a dramatic influence on particle behavior. This is because the effective viscosity is now a function of strain rate and there is a positive feedback effect, with strong particles hardening with decreasing strain rate and weak particles softening with increasing strain rate. For an initial effective viscosity ratio for particle to matrix of only 2, n_i for the inclusion of 6 (calcite) and n_m for the matrix of 3 (quartz), the inclusion behaves like an effectively rigid

particle, with the axial ratio R only reaching a value of 1.13 for $\gamma = 6$. It follows that the observed little deformed calcite clasts in the Neves area can be readily explained for quite low effective viscosity contrasts (on the order of 2) for the experimental range of stress exponents determined for coarse calcite and quartzite.

6. Discussion: Influence of Water on Flow in the Middle to Lower Crust

[31] The effectively rigid behavior of single-crystal calcite porphyroclasts, the lack of high-temperature twinning and the millimeter-sized subgrains and occasional recrystallized grains in the calcite, together with the millimeter-sized new grains in the surrounding quartz mylonites, developed by grain boundary migration, all indicate low flow stress in these shear zones. This is also consistent with the observation of Pennacchioni and Mancktelow [2007] that significant movement on these zones can occur even for very low resolved shear stress. The interpreted flow stress of <10 MPa for quartz-rich rocks under wet amphibolite facies conditions of $\sim 550^\circ\text{C}$ is more than an order of magnitude less than the values of 300–500 MPa inferred by Mancktelow and Pennacchioni [2004] and Fitz Gerald *et al.* [2006] for the flow and intermittent fracture of quartz-rich rocks under dry but otherwise similar metamorphic conditions in the Mont Mary unit of the Western Alps. The recrystallized grain size is correspondingly dramatically different: <30 μm (often with mantles of 2–5 μm) in the Mont Mary mylonites, whereas generally >1 mm in the Neves examples. Water is clearly the crucial factor, with a dramatic effect in quartz on the flow stress for dislocation creep and on the mobility of grain boundaries [e.g., Jaoul *et al.*, 1984; Paterson, 1989; Hirth *et al.*, 2001; Mancktelow and Pennacchioni, 2004; Rutter and Brodie, 2004b; Fitz Gerald *et al.*, 2006], but with no apparent effect on dislocation creep in calcite [de Bresser *et al.*, 2005; Rutter, 1974]. Middle to lower crust dominated by quartz-rich rocks is therefore either strong or weak during deformation depending on the availability of water. Old, polymetamorphic, dehydrated crust is strong whereas crust dominated by hydrous, previously unmetamorphosed and undeformed granitoid plutons, quartz-rich rocks and quartz veins, such as the ones studied here, are weak.

7. Conclusions

[32] The extrapolation of experimentally determined flow laws to natural ductile deformation in rocks is based on the assumption that flow parameters are constant with changing conditions and that parameters not included in the flow law have a negligible influence on the creep properties. The validity of this extrapolation to nature can only be tested, at least semiquantitatively, by comparison with naturally deformed rocks. Here we report for the first time direct field evidence that coarse calcite single crystals can be unequivocally stronger than polycrystalline quartz in natural shear zones developed under hydrous amphibolite facies conditions. Although the extrapolation of experimentally determined flow laws shows a rather wide spread, the generally lower strain rate dependence of coarse calcite compared to quartz is consistent with an inversion in their relative strength toward the lower strain rates expected in nature.

Predicted effective viscosity ratios are not high, but numerical modeling demonstrates that ratios ≥ 2 are sufficient to produce near rigid calcite clast behavior for power law stress exponents typically reported for coarse calcite (≥ 6) and quartz (3–4). In a sense, it is not so much that coarse calcite is strong but rather that wet quartzite is weak, with flow stress interpreted to be <10 MPa. Such low flow stresses for quartz-rich rocks in the granitic plutons of the Neves area, which were not significantly deformed or metamorphosed prior to the Alpine orogeny, reflects the water-rich amphibolite facies conditions. The low values are in marked contrast to the much higher differential stresses reported for the flow (and fracture) of quartz-rich rocks under dry conditions in the middle to lower crust.

[33] **Acknowledgments.** Constructive and insightful reviews by Hans de Bresser and Marco Herwegh are gratefully acknowledged. Bernardo Cesare and James Connolly are thanked for discussions on oxygen fugacity levels in the Neves mylonites, allowing a critical comparison with experimental data. The Matlab scripts for conversion from axial shortening to a more general strain geometry are based on ones from Ray Fletcher, who is gratefully acknowledged (any errors are those of the authors!). Bernd Leiss is warmly thanked for providing access to the X-ray texture goniometer at the Geoscience Centre of the University of Göttingen (Germany), for his assistance and training in its use, and for his help in data elaboration. This work was supported financially by internal research funds of the ETH Zurich and by the Fondazione Cassa di Risparmio di Padova e Rovigo (“progetti di Eccellenza”) in Padua.

References

- Anovitz, L. M., and E. J. Essene (1987), Phase-equilibria in the system $\text{CaCO}_3\text{-MgCO}_3\text{-FeCO}_3$, *J. Petrol.*, *28*(2), 389–414.
- Bestmann, M., D. Prior, and K. T. A. Veltkamp (2004), Development of single-crystal σ -shaped quartz porphyroclasts by dissolution-precipitation creep in a calcite marble shear zone, *J. Struct. Geol.*, *26*(5), 869–883, doi:10.1016/j.jsg.2003.10.003.
- Bhattacharya, A., L. Mohanty, A. Maji, S. K. Sen, and M. Raith (1992), Non-ideal mixing in the phlogopite-annite boundary: Constraints from experimental data on Mg-Fe partitioning and a reformulation of the biotite-garnet geothermometer, *Contrib. Mineral. Petrol.*, *111*(1), 87–93, doi:10.1007/BF00296580.
- Brodie, K. H., and E. H. Rutter (2000), Deformation mechanisms and rheology: Why marble is weaker than quartzite, *J. Geol. Soc.*, *157*(6), 1093–1096.
- Burkhard, M. (1993), Calcite twins, their geometry, appearance and significance as stress-strain markers and indicators of tectonic regime: A review, *J. Struct. Geol.*, *15*(3–5), 351–368, doi:10.1016/0191-8141(93)90132-T.
- Cesare, B., E. Poletti, M. C. Boiron, and M. Cathelineau (2001), Alpine metamorphism and veining in the Zentralgneis Complex of the SW Tauern Window: A model of fluid-rock interactions based on fluid inclusions, *Tectonophysics*, *336*(1–4), 121–136, doi:10.1016/S0040-1951(01)00097-X.
- Chernak, L. J., G. Hirth, J. Selverstone, and J. Tullis (2009), Effect of aqueous and carbonic fluids on the dislocation creep strength of quartz, *J. Geophys. Res.*, *114*, B04201, doi:10.1029/2008JB005884.
- Dasgupta, S., P. Sengupta, D. Guha, and M. Fukuda (1991), A refined garnet-biotite Fe–Mg exchange geothermometer and its application in amphibolites and granulites, *Contrib. Mineral. Petrol.*, *109*(1), 130–137, doi:10.1007/BF00687206.
- de Bresser, J. H. P. (2002), On the mechanism of dislocation creep of calcite at high temperature: Inferences from experimentally measured pressure sensitivity and strain rate sensitivity of flow stress, *J. Geophys. Res.*, *107*(B12), 2337, doi:10.1029/2002JB001812.
- de Bresser, J. H. P., and C. J. Spiers (1990), High-temperature deformation of calcite single crystals by r^+ and f^+ slip, in *Deformation Mechanisms, Rheology and Tectonics*, edited by R. J. Knipe and E. H. Rutter, *Geol. Soc. Spec. Publ.*, *54*, 285–298.
- de Bresser, J. H. P., and C. J. Spiers (1997), Strength characteristics of the r , f , and c slip systems in calcite, *Tectonophysics*, *272*(1), 1–23, doi:10.1016/S0040-1951(96)00273-9.
- de Bresser, J. H. P., J. L. Urai, and D. L. Olgaard (2005), Effect of water on the strength and microstructure of Carrara marble axially compressed at high temperature, *J. Struct. Geol.*, *27*(2), 265–281, doi:10.1016/j.jsg.2004.10.002.
- Delle Piane, C., L. Burlini, K. Kunze, P. Brack, and J. P. Burg (2008), Rheology of dolomite: Large strain torsion experiments and natural examples, *J. Struct. Geol.*, *30*(6), 767–776, doi:10.1016/j.jsg.2008.02.018.
- Eshelby, J. D. (1957), The determination of the elastic field of an ellipsoidal inclusion, and related problems, *Proc. R. Soc. London, Ser. A*, *241*, 376–396, doi:10.1098/rspa.1957.0133.
- Evans, B., and D. L. Kohlstedt (1995), Rheology of rocks, in *Rock Physics and Phase Relations: A Handbook of Physical Constants*, AGU Ref. Shelf, vol. 3, edited by T. Ahrens, pp. 148–165, AGU, Washington, D. C.
- Farver, J. R., and R. A. Yund (1991), Oxygen fugacity in quartz: Dependence on temperature and water fugacity, *Chem. Geol.*, *90*(1–2), 55–70, doi:10.1016/0009-2541(91)90033-N.
- Farver, J., and R. Yund (2000), Silicon diffusion in a natural quartz aggregate: Constraints on solution-transfer diffusion creep, *Tectonophysics*, *325*(3–4), 193–205, doi:10.1016/S0040-1951(00)00121-9.
- Ferrill, D. A. (1991), Calcite twin widths and intensities as metamorphic indicators in natural low-temperature deformation of limestone, *J. Struct. Geol.*, *13*, 667–675, doi:10.1016/0191-8141(91)90029-I.
- Ferrill, D. A. (1998), Critical re-evaluation of differential stress estimates from calcite twins in coarse-grained limestone, *Tectonophysics*, *285*(1–2), 77–86, doi:10.1016/S0040-1951(97)00190-X.
- Ferrill, D. A., A. P. Morris, M. A. Evans, M. Burkhard, R. H. J. Groshong, and C. A. Onasch (2004), Calcite twin morphology: A low-temperature deformation geothermometer, *J. Struct. Geol.*, *26*(8), 1521–1529, doi:10.1016/j.jsg.2003.11.028.
- Ferry, J. M., and F. S. Spear (1978), Experimental calibration of the partitioning of Fe and Mg between biotite and garnet, *Contrib. Mineral. Petrol.*, *66*(2), 113–117, doi:10.1007/BF00372150.
- Fitz Gerald, J. D., N. S. Mancktelow, G. Pennacchioni, and K. Kunze (2006), Ultrafine-grained quartz mylonites from high-grade shear zones: Evidence for strong dry middle to lower crust, *Geology*, *34*(5), 369–372, doi:10.1130/G22099.1.
- Freund, D., E. Rybacki, and G. Dresen (2001), Effect of impurities on grain growth in synthetic calcite aggregates, *Phys. Chem. Miner.*, *28*(10), 737–745, doi:10.1007/s002690100196.
- Ganguly, J., and S. K. Saxena (1984), Mixing properties of aluminosilicate garnets: Constraints from natural and experimental data, and applications to geothermo-barometry, *Am. Mineral.*, *69*(1–2), 88–97.
- Gleason, G. C., and J. Tullis (1995), A flow law for dislocation creep of quartz aggregates determined with the molten-salt cell, *Tectonophysics*, *247*(1–4), 1–23, doi:10.1016/0040-1951(95)00011-B.
- Goldman, D. S., and A. L. Albee (1977), Correlation of Mg/Fe partitioning between garnet and biotite with $^{18}\text{O}/^{16}\text{O}$ partitioning between quartz and magnetite, *Am. J. Sci.*, *277*(6), 750–767.
- Griggs, D. T. (1967), Hydrolytic weakening of quartz and other silicates, *Geophys. J. R. Astron. Soc.*, *14*(1–4), 19–31.
- Griggs, D. T., and J. D. Blacic (1965), Quartz: Anomalous weakness of synthetic crystals, *Science*, *147*(3655), 292–295, doi:10.1126/science.147.3655.292.
- Hansen, F. D., and N. L. Carter (1982), Creep of selected crustal rocks at 1000 MPa, *Eos Trans. AGU*, *63*, 437.
- Heard, H. C., and C. B. Raleigh (1972), Steady-state flow in marble at 500° to 800°C, *Geol. Soc. Am. Bull.*, *83*(4), 935–956, doi:10.1130/0016-7606(1972)83<935:SFIMAT>2.0.CO;2.
- Herwegh, M., X. H. Xiao, and B. Evans (2003), The effect of dissolved magnesium on diffusion creep in calcite, *Earth Planet. Sci. Lett.*, *212*, 457–470, doi:10.1016/S0012-821X(03)00284-X.
- Herwegh, M., J. H. P. de Bresser, and J. H. ter Heege (2005), Combining natural microstructures with composite flow laws: An improved approach for the extrapolation of lab data to nature, *J. Struct. Geol.*, *27*(3), 503–521, doi:10.1016/j.jsg.2004.10.010.
- Hirth, G., C. Teyssier, and W. J. Dunlap (2001), An evaluation of quartzite flow laws based on comparisons between experimentally and naturally deformed rocks, *Int. J. Earth Sci.*, *90*(1), 77–87, doi:10.1007/s005310000152.
- Hodges, K. V., and F. S. Spear (1982), Geothermometry, geobarometry and the Al_2SiO_5 triple point at Mt. Moosilauke, New Hampshire, *Am. Mineral.*, *67*(11), 1118–1134.
- Hoernes, S., and H. Friedrichsen (1974), Oxygen isotope studies on metamorphic rocks of the western Hohe Tauern area (Austria), *Schweiz. Mineral. Petrogr. Mitt.*, *54*, 769–788.
- Holdaway, M. J., and S. M. Lee (1977), Fe-Mg cordierite stability in high grade pelitic rocks based on experimental, theoretical and natural observations, *Contrib. Mineral. Petrol.*, *63*(2), 175–198, doi:10.1007/BF00398778.
- Indares, A., and J. Martignole (1985), Biotite-garnet thermometry in the granulite facies: The influence of Ti and Al in biotite, *Am. Mineral.*, *70*(3–4), 272–278.

- Jamison, W. R., and J. H. Spang (1976), Use of calcite twin lamellae to infer differential stress, *Geol. Soc. Am. Bull.*, 87(6), 868–872, doi:10.1130/0016-7606(1976)87<868:UOCTLT>2.0.CO;2.
- Jaoul, O., J. Tullis, and A. K. Kronenberg (1984), The effect of varying water contents on the creep behavior of Heavittree quartzite, *J. Geophys. Res.*, 89(B6), 4298–4312, doi:10.1029/JB089iB06p04298.
- Johnson, A. M., and R. C. Fletcher (1994), *Folding of Viscous Layers*, 461 pp., Columbia Univ. Press, New York.
- Koch, P. S., J. M. Christie, A. Ord, and R. P. George Jr. (1989), Effect of water on the rheology of experimentally deformed quartzite, *J. Geophys. Res.*, 94(B10), 13,975–13,996, doi:10.1029/JB094iB10p13975.
- Kohlstedt, D. L., B. Evans, and S. J. Mackwell (1995), Strength of the lithosphere: Constraints imposed by laboratory experiments, *J. Geophys. Res.*, 100(B9), 17,587–17,602, doi:10.1029/95JB01460.
- Kronenberg, A. K., and J. Tullis (1984), Flow strengths of quartz aggregates: Grain-size and pressure effects due to hydrolytic weakening, *J. Geophys. Res.*, 89(B6), 4281–4297, doi:10.1029/JB089iB06p04281.
- Lacombe, O., and P. Laurent (1996), Determination of deviatoric stress tensors based on inversion of calcite twin data from experimentally deformed monophase samples: Preliminary results, *Tectonophysics*, 255(3–4), 189–202, doi:10.1016/0040-1951(95)00136-0.
- Lavrent'eva, I. V., and L. L. Perchuk (1981), Phase correspondence in the system biotite-garnet: Experimental data, *Dokl. Akad. Nauk USSR*, 260, 731–734.
- Mancktelow, N. S. (2006), How ductile are ductile shear zones?, *Geology*, 34(5), 345–348, doi:10.1130/G22260.1.
- Mancktelow, N. S. (2008), Tectonic pressure: Theoretical concepts and modelled examples, *Lithos*, 103(1–2), 149–177, doi:10.1016/j.lithos.2007.09.013.
- Mancktelow, N. S., and G. Pennacchioni (2004), The influence of grain boundary fluids on the microstructure of quartz-feldspar mylonites, *J. Struct. Geol.*, 26(1), 47–69, doi:10.1016/S0191-8141(03)00081-6.
- Mancktelow, N. S., L. Arbaret, and G. Pennacchioni (2002), Experimental observations on the effect of interface slip on rotation and stabilisation of rigid particles in simple shear and a comparison with natural mylonites, *J. Struct. Geol.*, 24(3), 567–585, doi:10.1016/S0191-8141(01)00084-0.
- Mulchrone, K. F., and K. Walsh (2006), The motion of a non-rigid ellipse in a general 2D deformation, *J. Struct. Geol.*, 28(3), 392–407, doi:10.1016/j.jsg.2005.12.008.
- Passchier, C. W., and C. Simpson (1986), Porphyroclast systems as kinematic indicators, *J. Struct. Geol.*, 8(8), 831–843, doi:10.1016/0191-8141(86)90029-5.
- Paterson, M. S. (1987), Problems in the extrapolation of laboratory rheological data, *Tectonophysics*, 133(1–2), 33–43, doi:10.1016/0040-1951(87)90278-2.
- Paterson, M. S. (1989), The interaction of water with quartz and its influence in dislocation flow—An overview, in *Rheology of Solids and of the Earth*, edited by S.-I. Karato and M. Toriumi, pp. 107–142, Oxford Sci., Oxford, U. K.
- Paterson, M. S., and F. C. Luan (1990), Quartzite rheology under geological conditions, in *Deformation Mechanisms, Rheology and Tectonics*, edited by R. J. Knipe and E. H. Rutter, *Geol. Soc. Spec. Publ.*, 54, 299–307.
- Pennacchioni, G., and N. S. Mancktelow (2007), Nucleation and initial growth of a shear zone network within compositionally and structurally heterogeneous granulites under amphibolite facies conditions, *J. Struct. Geol.*, 29(11), 1757–1780, doi:10.1016/j.jsg.2007.06.002.
- Pennacchioni, G., G. Di Toro, and N. S. Mancktelow (2001), Strain-insensitive preferred orientation of porphyroclasts in Mont Mary mylonites, *J. Struct. Geol.*, 23(8), 1281–1298, doi:10.1016/S0191-8141(00)00189-9.
- Perchuk, L. L., and I. V. Lavrent'eva (1983), Experimental investigation of exchange equilibria in the system cordierite-garnet-biotite, in *Kinetics and Equilibrium in Mineral Reactions*, edited by S. K. Saxena, pp. 199–239, Springer, New York.
- Perchuk, L. L., K. K. Podlesskii, and L. Y. Aronvich (1981), Calculations of thermodynamic properties of end-member minerals from natural paragenesis, in *Thermodynamics of Minerals and Melts*, edited by R. C. Newton, A. Navrotsky, and B. J. Woods, pp. 111–129, Springer, Heidelberg, Germany.
- Pfiffner, O. A., and J. G. Ramsay (1982), Constraints on geological strain rates: Arguments from finite strain states of naturally deformed rocks, *J. Geophys. Res.*, 87(B1), 311–321, doi:10.1029/JB087iB01p00311.
- Pieri, M., L. Burlini, K. Kunze, I. Stretton, and D. L. Olgaard (2001), Rheological and microstructural evolution of Carrara marble with high shear strain: Results from high temperature torsion experiments, *J. Struct. Geol.*, 23(9), 1393–1413, doi:10.1016/S0191-8141(01)00006-2.
- Pigage, L. C., and H. J. Greenwood (1982), Internally consistent estimates of pressure and temperature: The staurolite problem, *Am. J. Sci.*, 282(7), 943–969.
- Poirier, J. P. (1985), *Creep of Crystals*, 260 pp., Cambridge Univ. Press, Cambridge, U. K.
- Post, A. D., J. Tullis, and R. A. Yund (1996), Effects of chemical environment on dislocation creep of quartzite, *J. Geophys. Res.*, 101(B10), 22,143–22,155, doi:10.1029/96JB01926.
- Ranalli, G. (1987), *Rheology of the Earth*, 1st ed., 366 pp., Allen and Unwin, London.
- Rao, D. R. (1995), BGT—The macros driven spreadsheet program for biotite-garnet thermometry, *Comput. Geosci.*, 21(4), 593–604, doi:10.1016/0098-3004(94)00098-F.
- Renner, J., B. Evans, and G. Siddiqi (2002), Dislocation creep of calcite, *J. Geophys. Res.*, 107(B12), 2364, doi:10.1029/2001JB001680.
- Rowe, K. J., and E. H. Rutter (1990), Palaeostress estimation using calcite twinning: Experimental calibration and application to nature, *J. Struct. Geol.*, 12(1), 1–17, doi:10.1016/0191-8141(90)90044-Y.
- Rutter, E. H. (1974), The influence of temperature, strain rate and interstitial water in the experimental deformation of calcite rocks, *Tectonophysics*, 22, 311–334, doi:10.1016/0040-1951(74)90089-4.
- Rutter, E. H. (1995), Experimental study of the influence of stress, temperature, and strain on the dynamic recrystallization of Carrara marble, *J. Geophys. Res.*, 100(B12), 24,651–24,663, doi:10.1029/95JB02500.
- Rutter, E. H., and K. H. Brodie (2004a), Experimental grain size-sensitive flow of hot-pressed Brazilian quartz aggregates, *J. Struct. Geol.*, 26(11), 2011–2023, doi:10.1016/j.jsg.2004.04.006.
- Rutter, E. H., and K. H. Brodie (2004b), Experimental intracrystalline plastic flow in hot-pressed synthetic quartzite prepared from Brazilian quartz crystals, *J. Struct. Geol.*, 26(2), 259–270, doi:10.1016/S0191-8141(03)00096-8.
- Sassier, C., P. H. Leloup, D. Rubatto, O. Galland, Y. Yue, and D. Lin (2009), Direct measurement of strain rates in ductile shear zones: A new method based on syntectonic dikes, *J. Geophys. Res.*, 114, B01406, doi:10.1029/2008JB005597.
- Schmid, D. W., and Y. Y. Podladchikov (2003), Analytical solutions for deformable elliptical inclusions in general shear, *Geophys. J. Int.*, 155, 269–288, doi:10.1046/j.1365-246X.2003.02042.x.
- Schmid, S. M., and M. Casey (1986), Complete fabric analysis of some commonly observed quartz c-axis patterns, in *Mineral and Rock Deformation: Laboratory Studies: The Paterson Volume*, *Geophys. Monogr. Ser.*, vol. 36, edited by B. E. Hobbs and H. C. Heard, pp. 263–286, AGU, Washington, D. C.
- Schmid, S. M., M. S. Paterson, and J. N. Boland (1980), High temperature flow and dynamic recrystallization in Carrara marble, *Tectonophysics*, 65(3–4), 245–280, doi:10.1016/0040-1951(80)90077-3.
- Schmid, S. M., R. Panozzo, and S. Bauer (1987), Simple shear experiments on calcite rocks: Rheology and microfabric, *J. Struct. Geol.*, 9(5–6), 747–778, doi:10.1016/0191-8141(87)90157-X.
- Stipp, M., and J. Tullis (2003), The recrystallized grain size piezometer for quartz, *Geophys. Res. Lett.*, 30(21), 2088, doi:10.1029/2003GL018444.
- Stipp, M., H. Stunitz, R. Heilbronner, and S. M. Schmid (2002), The eastern Tonale fault zone: A 'natural laboratory' for crystal plastic deformation of quartz over a temperature range from 250 to 700°C, *J. Struct. Geol.*, 24(12), 1861–1884, doi:10.1016/S0191-8141(02)00035-4.
- Stipp, M., J. Tullis, and H. Behrens (2006), Effect of water on the dislocation creep microstructure and flow stress of quartz and implications for the recrystallized grain size piezometer, *J. Geophys. Res.*, 111(B4), B04201, doi:10.1029/2005JB003852.
- Thomson, A. B. (1976), Mineral reaction in polytic rocks. Calculation of some P-T-X (Fe-Mg) phase relations, *Am. J. Sci.*, 276(4), 425–454.
- Tödheide, K. (1972), Water at high temperatures and pressures, in *Water: A Comprehensive Treatise*, edited by F. Franks, pp. 463–514, Plenum, New York.
- Tullis, J., and R. A. Yund (1989), Hydrolytic weakening of quartz aggregates: The effects of water and pressure on recovery, *Geophys. Res. Lett.*, 16(11), 1343–1346, doi:10.1029/GL016011p01343.
- Tullis, T. E. (1980), The use of mechanical twinning in minerals as a measure of shear stress magnitudes, *J. Geophys. Res.*, 85(B11), 6263–6268, doi:10.1029/JB085iB11p06263.
- Turner, F. J., D. T. Griggs, and H. C. Heard (1954), Experimental deformation of calcite crystals, *Geol. Soc. Am. Bull.*, 65(9), 883–934, doi:10.1130/0016-7606(1954)65[883:EDOC]2.0.CO;2.
- Urai, J. L., W. D. Means, and G. S. Lister (1986), Dynamic recrystallization of minerals, in *Mineral and Rock Deformation: Laboratory Studies: The Paterson Volume*, *Geophys. Monogr. Ser.*, vol. 36, edited by B. E. Hobbs and H. C. Heard, pp. 161–191, AGU, Washington, D. C.
- Wang, Z.-C., Q. Bai, G. Dresen, and R. Wirth (1996), High-temperature deformation of calcite single crystals, *J. Geophys. Res.*, 101(B9), 20,377–20,390, doi:10.1029/96JB01186.
- Weertman, J. (1955), Theory of steady-state creep based on dislocation climb, *J. Appl. Phys.*, 26(10), 1213–1217, doi:10.1063/1.1721875.
- Weertman, J. (1968), Dislocation climb theory of steady-state creep, *Q. Trans. Am. Soc. Metals*, 61(4), 681–694.

Williams, M. L., and J. A. Grambling (1990), Manganese, ferric iron, and the equilibrium between garnet and biotite, *Am. Mineral.*, 75(7–8), 886–908.

Xu, L., J. Renner, M. Herwegh, and B. Evans (2009), The effect of dissolved magnesium on creep of calcite II: Transition from diffusion creep

to dislocation creep, *Contrib. Mineral. Petrol.*, 157(3), 339–358, doi:10.1007/s00410-008-0338-5.

N. S. Mancktelow, Department of Earth Sciences, ETH Zurich, Sonneggstrasse 5, CH-8092 Zurich, Switzerland. (mancktelow@erdw.ethz.ch)

G. Pennacchioni, Department of Geosciences, University of Padua, I-35137 Padua, Italy.